EFFECTS OF PARAMAGNETIC MINERALS ON PORE-SIZE DISTRIBUTION IN SHALE

By

CHRISTIAN CHIJINDU OBASI

Bachelor of Science in Geology
University of Nigeria, Nsukka
Enugu, Nigeria
2003

Master of Science in Stratigraphy and Inorganic Geochemistry.
Temple University
Philadelphia, Pennsylvania
2008

Submitted to the Faculty of the
Graduate College of the
Oklahoma State University
in partial fulfillment of
the requirements for
the Degree of
DOCTOR OF PHILOSOPHY
December, 2018

EFFECTS OF PARAMAGNETIC MINERALS ON

PORE-SIZE DISTRIBUTION IN SHALE

Dissertation Approved:

Dr. Jack Pashin

Dissertation Adviser

Dr. Michael Grammer

Dr. Javier Vilcaez

Dr. Toby Nelson

ACKNOWLEDGEMENTS

I would like to thank my advisor, Dr. Jack Pashin, for assisting and mentoring me through this process; and for providing insightful feedback on my work. I would also like to thank my committee members, Dr. Michael Grammer, Dr. Javier Vilcaez and Dr. Toby Nelson for their support to this thesis.

I would like to acknowledge all faculty, students and staff members of Oklahoma State University, Boone Pickens School of Geology, with whom I interacted and benefitted from their generosity, guidance and advice on related and non-related dissertation matters. I would like to thank Dr. Pashin and the Boone Pickens School of Geology providing the funds via research fund and "student enrichment fund", for my research materials and travel to Rutgers University for my Nuclear Magnetic Resonance laboratory analyses, respectively. I would like to also thank the Alumni of the Boone Pickens School of Geology for the partial award granted to me via the graduate alumni fellowship. I would like to thank all the graduate students of Boone Pickens School of Geology, past or present, particularly Leye Adeboye, Dr. Abongwa and Jenny Meng.

I would like to specifically thank Dr. Kristina Keating and her team; Gordon, Samuel, Judy and Toni, at Rutgers University Newark, for the guidance in preparing and running my Nuclear Magnetic Resonance laboratory analyses at Dr. Keating's laboratory. I would also like to thank Dr. Jim Puckette of Oklahoma State University, Boone Pickens School of Geology for the use of his core-laboratory and X-ray Fluorescence equipment.

I would like to thank Dr. Keating and the anonymous reviewers for their insightful comments and suggestions that have made the publications of the manuscript in this thesis stronger.

Finally, I would like to thank my family for their prayers, encouragement, and support; spiritually, financially and morally through this process. My siblings Chidinma, Wilfred, Emmanuel, Onyeka, Maureen, Stella and Ngozi, thank you guys. I would like to thank my parents, Elder Wilfred N. and Mrs. Mary, Obasi for keeping me grounded; this Ph.D. degree is dedicated to you daddy.

Most of all, I would like to thank my queen, my wife and the love of my world, Naa Obasi, for being a true lover, partner and mother, tolerating the very long working hours, and at one time, long four weeks away from home. My children Jesse, Kristina, and the ones unborn, I love you dearly and pray that you will surpass my achievements in life.

TABLE OF CONTENTS

.

LIST OF FIGURES

LIST OF TABLES

CHAPTER 1

THESIS OVERVIEW

1. 1 Motivation

The proliferation of hydrocarbon production from unconventional reservoirs has led to increased interest into the reservoir properties of shale. Proton nuclear magnetic resonance, NMR relaxation has been used to detect the presence of hydrogen nuclei in medical science for medical Magnetic Resonance Imaging (MRI), and in earth sciences to explore and appraise groundwater and petroleum resources. In earth science, NMR measurements can be obtained in the laboratory or in the field via well-logging as a valuable tool for determining pore-size distribution based on the distribution of relaxation times (Kenyon et al., 1995; Latour et al., 1995; Hürlimann et al., 2004), from which reservoir properties such as porosity, permeability, bound water content, free fluid content and total saturation can be derived (Kleinberg, 1994; Allen et al., 2000). The advantages of NMR over other wireline surveys are that it can yield a continuous log of permeability, can provide lithology-independent porosity, is non-invasive and does not require radioactive source (Kenyon et al., 1995; Daughney et al., 2000; Westphal et al., 2005; Washburn, 2014).

Interpretation of NMR logs, which are used to assess fluid saturation and mobility, from microporous shale reservoirs is a challenge for unconventional oil and gas exploration because it was developed for the characterization of macroporous sandstone and carbonate reservoirs and is not always accurate in shale. The partitioning of transverse relaxation time (T_2) distribution into irreducible and mobile fluids using a T_2-cutoff value is standard practice. However, in shale this approach does not always yield accurate results due to high clay contents, differential compaction, and magnetic minerals that can strongly influence the NMR log response.

In porous media, effects of internal gradient caused by magnetic susceptibility contrast between the matrix and infilling fluid shifts transverse relaxation (T_2) to shorter time, resulting in imprecise classification of pore-sizes. In shale, details of the effects of paramagnetic and clay minerals that induce the internal gradients, are poorly understood.

1.2 Problems, Hypothesis and Objectives

The goal of this research was to interpret the effects of paramagnetic minerals on the determination of pore-size distribution in shale using NMR and the implications for estimating permeability.

The hypotheses tested were:

(1) The internal magnetic field gradients that occur due to the presence of magnetic and paramagnetic minerals common in shale.

(2) Incrementally compacting and increasing the concentrations of the mineral constituents of shale to identify the controlling mechanisms for NMR transverse relaxation.

(3) Application of the effects of internal magnetic field gradients and compaction on pore-size distribution in the Woodford Shale core.

The objectives of this study were:

(1) To determine the effects of magnetic minerals on pore-size distribution in shale.

(2) To determine the effect of incremental compaction of magnetic minerals common in shale, on NMR transverse relaxation time, T_2.

(3) To analyze the effects of internal magnetic field gradient and compaction on Woodford Shale reservoir properties.

The hypotheses were tested and the project objectives met by using a granular form of minerals, including kaolinite, montmorillonite, glauconite, illite, pyrite, celadonite, chamosite, mixed with 125 g/L brine, to infer contributions of each to T_2 relaxation in shale. The outcome of these studies was applied to enhance the petrophysical interpretation of the Woodford shale core.

1.3 Significance

The understanding of the effects of internal gradients in shale is important to quantify the shortening of T_{2ML}, which leads to overestimation of bulk fluid volume (*BFV*) and, thus, underestimating NMR permeability when used as an input into permeability estimator equations. The workflow from this research can be integrated with traditional petrophysical methods, to gain useful insight into petrophysical interpretations of various unconventional reservoir rocks.

REFERENCES CITED

Allen, D., Flaum, C., Ramakrishnan, T., Bedford, J., Castelijns, K., Fairhurst, D., Gubelin, G., Heaton, N., Minh, C. C., and Norville, M. A., 2000, Trends in NMR logging: Oilfield Review, v. 12, no. 3, p. 2-19.

Daughney, C. J., Bryar, T. R., and Knight, R. J., 2000, Detecting sorbed hydrocarbons in a porous medium using proton nuclear magnetic resonance: Environmental science & technology, v. 34, no. 2, p. 332-337

Hu¨rlimann, M. D., A. Matteson, J. Massey, D. Allen, E. Fordham, F. Antonsen, and H. Ruesla¨tten, 2004, Application of NMR diffusion editing as chlorite indicator: Petrophysics, v. 45, p. 414–421.

Kenyon, B., R. Kleinberg, C. Straley, G. Gubelin, and C. Morriss, 1995, Nuclear magnetic resonance imaging— Technology for the 21st century: Oilfield Review, v. 7, p. 19–33.

Kleinberg, R. L., W. E. Kenyon, and P. P. Mitra, 1994, Mechanism of NMR relaxation of fluids in rock: Journal of Magnetic Resonance. Series A., v. 108, no. 2, p. 206–214, doi:10.1006/jmra.1994.1112.

Latour, L., Kleinberg, R. L., Mitra, P. P., and Sotak, C. H., 1995, Pore-size distributions and tortuosity in heterogeneous porous media: Journal of Magnetic Resonance, Series A, v. 112, no. 1, p. 83-91.Washburn, K. E., 2014, Relaxation mechanisms and shales: Concepts in Magnetic Resonance Part A, v. 43A, no. 3, p. 57–78, doi:10.1002/cmr.a.21302.

Washburn, K. E., 2014, Relaxation mechanisms and shales: Concepts in Magnetic Resonance Part A, v. 43, no. 3, p. 57-78.

Westphal, H., Surholt, I., Kiesl, C., Thern, H. F., and Kruspe, T., 2005, NMR measurements in carbonate rocks: Problems and an approach to a solution: Pure and Applied Geophysics, v. 162, no. 3, p. 549-570.

CHAPTER 2

EFFECTS OF INTERNAL GRADIENTS ON PORE-SIZE DISTRIBUTION IN SHALE

Obasi and Pashin 2018

American Association of Petroleum Geologists Bulletin (DOI: 10.1306/02271816507)

Boone Pickens School of Geology, Oklahoma State University, 105 Noble Research Center, Stillwater, OK 74078-3031.

ABSTRACT:

In porous media, effects of internal gradient caused by magnetic susceptibility contrast between the matrix and infilling fluid shifts transverse relaxation (T_2) to shorter time, resulting in imprecise classification of pore-sizes. In shale, details of the effects of paramagnetic and clay minerals that induce the internal gradients, are poorly understood. We measured a brine mixture with a granular form of minerals, including kaolinite, montmorillonite, glauconite, illite, pyrite, celadonite, and chamosite, to infer contributions of each to T_2 relaxation in shale. Nuclear magnetic resonance (NMR

response of these samples was used to calculate the total mean logarithm of T_2 (T_{2ML}) and volume of water in the samples. Additionally, physical properties such as magnetic susceptibility, specific surface area, and elemental composition were acquired. Pore geometry, magnitude of internal gradients, pore-size distributions, and secular regimes in which the media relaxed (based on their shortest characteristic time scales) were characterized from these properties. These time scales measure the behavior of the relaxation regimes such as longitudinal relaxation time-to-T_2 ratio and dependence of relaxation rate on echo spacing (t_E). Glauconite illite, pyrite, chamosite, and kaolinite grouped into a small-pore system, whereas montmorillonite and celadonite grouped into large-pores system. A free diffusion regime governed secular relaxation for kaolinite; a motional-averaging regime governed montmorillonite, celadonite and large t_E chamosite; whereas a localization regime dominated the rest minerals. We conclude that understanding the effects of internal gradients in shale is important to quantify the shortening of T_{2ML}, which leads to overestimation of bulk fluid volume (*BFV*) and, thus, underestimating NMR permeability when used as an input into permeability estimator equations.

2.1 INTRODUCTION

The proliferation of hydrocarbon production from unconventional reservoirs has led to increased interest into the reservoir properties of shale. Proton nuclear magnetic resonance (NMR) relaxation has been used to detect the presence of hydrogen nuclei in medical science for medical magnetic resonance imaging and in earth sciences to explore

and appraise groundwater and petroleum resources. In earth science, NMR measurements can be obtained in the laboratory or in the field via well-logging techniques to determine rock porosity, pore-size distribution, and permeability (Keating and Knight, 2007). The NMR measurement in shale is more problematic than in sandstone or carbonate because of small pore size, low permeability (nanodarcy-microdarcy), and paramagnetic mineral components (Loucks et al., 2009; Washburn, 2014).

In petrophysical studies, the NMR relaxation measurement involves placing a fluid-saturated porous medium in the presence of static magnetic field. The magnetic moments of hydrogen nuclei (proton) in the fluid steadily precess or spin around the static magnetic field. An oscillating magnetic field is then applied to perturb the proton away from the static magnetic field. Once the oscillating field is removed, the NMR signal relaxes to equilibrium via two different simultaneous mechanisms. Insight into porous systems and saturating fluids can be gained by observing these two mechanisms (Washburn et al., 2013). The first is the time taken for the perturbed magnetization to relax to thermal equilibrium along the static magnetic field and is known as the longitudinal relaxation time (T_1). The second mechanism refers to the time taken for spins to decay to a completely disordered state and reach equilibrium among themselves from a highly ordered state, and is known as transverse relaxation time (T_2) (Levitt, 2008; Keating and Knight, 2010; Washburn et al., 2013). In principle, T_1 and T_2 relaxation rates (inverse of T_1 and T_2 times) experience bulk relaxation from dipole-dipole molecular interactions and surface relaxation because of interactions between paramagnetic sites at the pore surface and the pore-fluid protons. Transverse relaxation time alone is affected by diffusion relaxation, which is sensitive to variations in magnetic fields between the

rock matrix and the pore fluid (Bloembergen et al., 1948; Kenyon, 1997; Washburn and Birdwell, 2013 Washburn, 2014).

The application of NMR to extract information about pore-size distribution, porosity, and permeability from porous media, such as sedimentary rocks, is strongly affected by the presence of paramagnetic materials (Hürlimann, 1998; Bryar et. al., 2000). Paramagnetic materials complicate comparisons among materials with varying paramagnetic content and are a substantial source of error in pore size calculations (Bryar et. al., 2000). When a porous material is placed in a homogeneous magnetic field during NMR measurement, the magnetic susceptibility contrast between the solid matrix and the pore fluid induces magnetic field inhomogeneity in the pore space (Hürlimann, 1998). Inhomogeneity in the magnetic field increases the relaxation rate, creating additional transverse relaxation term, as a function of echo spacing (t_E) (Anand and Hirasaki, 2008). For example, T_2 is shortened when chlorite, a paramagnetic mineral is present in sandstone and shale, because of the large internal magnetic field gradient it creates, (Rueslåtten et al., 1998; G. Q. Zhang et al., 1998). The magnitude of the shortened T_2 is defined as secular relaxation (Anand and Hirasaki, 2008), which is expressed as

$$\frac{1}{T_{2,sec}} = \frac{1}{T_1} - \frac{1}{T_2}, \tag{1}$$

where $T_{2,\mathrm{sec}}$ is secular relaxation time. The shortened T_2 creates bias in pore-size distribution in shale that is proportional to $T_{2,sec}$. Estimating permeability with NMR relies on the ability to use T_2 to calculate irreducible and mobile fluid saturations using a T_2 cutoff value. Ultimately, this approach makes assumptions about the way that irreducible water resides in small pores and mobile fluid resides in large pores (Chen et al., 1998; Coates et al., 1998). So when bound fluid volume (BFV), free fluid volume,

and T_2 logarithmic mean relaxation time are used as input into either of the two widely used permeability estimators; 1) Timur-Coates estimator, (Timur, 1968a, b, 1969 Coates and Dumanoir, 1973; Sezginer et al., 1999; Allen et al., 2001) and (2) the Schlumberger-Doll Research (SDR) estimator (Kenyon et al., 1988; Sezginer et al., 1999; Allen et al., 2001) which overestimate BFV and T_2 logarithmic mean relaxation time while underestimating permeability (G. Q. Zhang et al., 1998; Hürlimann et al., 2004)

This research is designed to interpret the effects of paramagnetic minerals on the determination of pore-size distribution in shale using NMR and the implications for estimating permeability. This research focuses on measuring the internal magnetic field gradients that occur as a result of the presence of magnetic and paramagnetic minerals common in shale. The working hypothesis is that the magnitude of internal magnetic field gradient in shale is caused by contributions from constituent minerals, and this creates secular relaxation, which introduces error in NMR-based estimation of pore-size distribution and permeability. This hypothesis was tested in an experiment designed to determine the magnitude of the internal magnetic field gradients in the pore spaces of mineral/brine mixtures using the methods of Kleinberg and Vinegar (1996), G. Q. Zhang et al. (1998), and Washburn (2014). Secular relaxation regimes that dominate the transverse T_2 relaxation distribution in the mixtures was computed using the approach of Anand and Hirasaki (2008) to demonstrate the impact of internal magnetic field gradients on the T_2 logarithmic mean relaxation and pore-size distribution. A recent study by Saidian et al. (2015) explored a methodology that correlated effects of paramagnetic clay content on surface relaxivity in organic-rich shales. However, our study's uniqueness is

that it directly examines the effects of constituent minerals, including various paramagnetic minerals, on transverse relaxation time in shale.

2.2 THEORY AND BACKGROUND

2.2.1 NMR Relaxation Theory

A summary of the governing principle of NMR theory is presented here; a comprehensive review of proton NMR relaxation theory is presented in Bloembergen et al. (1948); Kleinberg et al. (1994); Kenyon (1997); Coates et al., 1999, and Dunn et al. (2002). The mean relaxation rates, $T_{1,2ML}$ (second) distribution, assuming a case of fast diffusion limit for a single pore (Senturia and Robinson, 1970; Brownstein and Tarr, 1979; Keating and Knight, 2007) are given by

$$T_{1ML}^{-1} = T_{1B}^{-1} + \rho_1 \left(\frac{S}{V}\right) \tag{2}$$

$$T_{2ML}^{-1} = T_{2B}^{-1} + \rho_2 \left(\frac{S}{V}\right) + \frac{D}{12} (\gamma G t_E)^2 \tag{3}$$

Here, $T_{1,2B}^{-1}$ (s^{-1}) is the relaxation rate of the bulk water, $\rho_{1,2}$ (micrometers per second) is the surface relaxivity, γ (42.58 MHz/*T*esla) is the gyromagnetic ratio of the hydrogen proton, D is the self-diffusion coefficient (D = 2.46 x 10^{-9} m^2/s), $\frac{S}{V}$ (1/μm) is the surface-area-to-volume ratio (inversely proportional to the pore radius r_{pore}), t_E is in milliseconds, and G (in gauss per centimeter or Tesla per meter) is the average gradient strength of static magnetic field. In general, T_1 measurements are challenging with borehole or surface instruments because they have longer measurement times than T_2, and are poorly repeatable when logging past bed boundaries (Kleinberg et al., 1993b;

LaTorraca et al., 1995; Kleinberg and Vinegar, 1996; Bachman et al., 2007; Grunewald and Knight, 2009). Therefore, T_2 measurements are typically central to NMR field applications and will be the focus in this paper.

In geologic materials with low magnetic susceptibility, surface relaxation dominates and the expression for T_2^{-1} (s^{-1}) is reduced to (per Grunewald and Knight, 2009),

$$T_2^{-1} = \rho_2 \left(\frac{S}{V}\right). \quad (4)$$

The diffusion relaxation rate, T_{2D}^{-1} (s^{-1}) is determined when relaxing protons diffuse and dephase in nonuniform magnetic field (Keating and Knight, 2010). In the unrestricted diffusion regime, T_{2D}^{-1} is described by Carr and Purcell (1954), Kleinberg and Horsfield (1990), Anand and Hirasaki (2008), Keating and Knight (2010), and as

$$T_{2D}^{-1} = \frac{D}{12} (\gamma G t_E)^2 \quad (5)$$

The Carr-Purcell-Meiboom-Gill (CPMG) pulse sequence was developed to refocus proton spins in a solid in the presence of internal gradients (Carr and Purcell, 1954; Meiboom and Gill, 1958; Keating and Knight, 2008, 2010). Rephasing of the spins in internal gradients, at the CPMG t_E, is imperfect because the dephasing is irreversible and the molecular motion is random, thus enhancing relaxation (Kleinberg and Vinegar, 1996).

The NMR relaxation response in a single water filled pore is such that the transverse magnetization signal is expressed by an exponential decay:

$$M(t) = A\, exp^{-t/T_2}, \quad (6)$$

Here A is the initial amplitude and is proportional to the number of hydrogen nuclei (related directly to the pore volume), and M is the bulk nuclear magnetization as a

function of time, *t*. In a sediment with different pore types, the conventional assumption is that the observed NMR signal is the sum of contributions from isolated individual pores, (each pore decaying independently) and the NMR signal is modeled as a multiexponential decay,

$$M(t) = \sum_i A_i \, exp\left(\frac{-t}{T_{2i}}\right), \tag{7}$$

Here, A_i is proportional to the protons in ith size pores relaxing with $1/T_{2i}$ relaxation rate. $M(t)$ data are inverted to obtain a T_{2i} distribution, which, assuming simple pore geometry and uniform surface relaxivity, can be scaled according to estimate pore size distribution (e.g., $S/V = 3/r_{pore}$ for planar pores).

Brownstein and Tarr (1979) proposed three ideal pore geometries for disordered porous media such as sedimentary rocks as spherical, cylindrical and planar. Likewise, they demonstrated that a single pore with an ideal pore shape, in fast diffusion regime, is $S_{por\text{-}i} = \alpha/r_i$ where $S_{por\text{-}i}$ and r_i are the surface-area-to-volume ratio and characteristic radius of the i^{th} pore respectively. α is a factor that accounts for the shape of the pore (α is 3, 2, and 1 for spherical, cylindrical and planar pores respectively) (Brownstein and Tarr, 1979; Costabel and Yaramanci, 2013; Keating, 2014). Keating and Knight (2008) determined pore surface-area-to-volume ratio, S_{por} by

$$S_{por} = \frac{S}{V} = \frac{S_S m_s}{V_w} \tag{8}$$

where m_s (grams) is the mass of the sample, S_s (square meters per gram) is the specific surface area normalized by the sample mass and V_w (milliliters) is the volume of water in the sample, which also represents the pore space volume V (Keating and Knight, 2010).

2.2.2 Longitudinal Relaxation Time to Transverse Relaxation Time Correlation

The T_1/T_2 correlation is an important tool in the study of molecular relaxation mechanism (Kleinberg and Horsfield, 1990; Song et al., 2002; Anand and Hirasaki, 2008). A T_1/T_2 ratio greater than one, for a nonviscous, single fluid system, may indicates the presence of magnetic field inhomogeneities in a porous media and the dependence of the relaxation on the t_E (Kleinberg et al., 1993a, b; Foley et al., 1996; Anand and Hirasaki, 2008). The mean value of T_1/T_2 ratio for most sandstone and carbonate rocks is 1.65 (Kleinberg et al., 1993a, b; Kleinberg and Vinegar, 1996). The technique for determining T_1/T_2 correlation map, which was applied in this study, has been described in Song et al. (2002).

Echo-spacing dependence underscores the significance of molecular diffusion mechanism (Kleinberg et al., 1993a). The dependence of T_2 on t_E reflects the strength of the internal magnetic field gradient (G. Q. Zhang et al., 1998). Diffusion relaxation is important when the coefficient of diffusion is high, that is,. at high temperature for water, gas or light hydrocarbons, or when t_E is large (Kleinberg and Vinegar, 1996). A plot of T_{2ML}^{-1} versus t_E^2 will generate a straight with a slope equal to $\frac{D(\gamma G)^2}{12}$; and if positive slope, indicates the presence of internal gradient (because of magnetic susceptibility contrasts) (i.e. $G \neq 0$) (Anand and Hirasaki, 2008; Keating and Knight, 2008; Keating, 2014)

2.2.3 Iron Content, Magnetic Susceptibilities and Paramagnetic Minerals

Sediments and sedimentary rocks have concentrations of iron ranging from less than 0.1% to greater than 10% (Cornell and Schwertmann, 2003).

Volume magnetic susceptibility, χ, of materials such as minerals common in shale, including chamosite, glauconite, kaolinite, montmorillonite, celadonite, illite, and pyrite, describes how readily the materials develop magnetic moment when exposed to an external magnetic field. χ is dimensionless and if a rock possesses positive χ value, it is paramagnetic else; it is called diamagnetic if it possesses negative χ value (Levitt, 2008). Iron-free minerals can have negative magnetic susceptibility χ, values and are diamagnetic (G. Q. Zhang et al., 1998).

2.2.4 External versus Internal Gradients

The maximal effective internal magnetic field gradient, $G_{\max}$ often referred to as "internal gradient" is the field inhomogeneity induced in the pore space because of the magnetic susceptibility contrast between the solid matrix and the pore fluid. The magnitude of internal magnetic field gradients can be expressed as follows (Kleinberg and Vinegar, 1996; G. Q. Zhang et al., 1998; Dunn et al., 2002; Washburn, 2014):

$$G_{max} = \frac{\Delta\chi B_0}{L} \quad (9)$$

Here, $\Delta\chi$ is magnetic susceptibility contrast between the pore fluid and grain matrix, B_0 is the strength of the applied static magnetic field ($B_0 = 0.0470\ Tesla\ or\ 470\ gauss$) and L (centimeters) is the distance of variation of the magnetic field.

Insight into typical sizes of internal gradients G_{max}, (in gauss per centimeter) in clays and some sedimentary rocks has been obtained in recent studies. Hürlimann (1998)

obtained G_{max} at 2 MHz in sandstones up to 1000 gauss/cm and as low as 0.5 gauss/cm in most carbonates (negligible compared to tool gradient). G. Q. Zhang et al. (1998) obtained approximately 711 and 1.8 gauss/cm for Chlorite-brine and kaolinite-brine slurries, respectively. However, the effects of these internal gradients are negligible if the static tool gradient (external gradient) of commercial logging tools dominates the total gradient in the pore space, when estimating the diffusion coefficient of the unknown fluids (Akkurt et al., 1995; Hürlimann, 1998). One of these commercial NMR logging tools presently available in the industry have peak external gradient of 20 gauss/cm over the sample volume and another has uniform external gradient of approximately 17 gauss/cm (Kleinberg and Vinegar, 1996; Kenyon, 1997). The 2-MHz Magritek Rock Core Analyzer used in this research has a static gradient strength at greater than 10 gauss/cm.

2.2.5 Secular Relaxation, Relaxation Regimes, and Characteristic Time Scales

The details of the governing principles of characteristic time scales, relaxation regimes and secular relaxations are in the referenced papers. Here we present a summary of equations and the approach relevant to our data preparation and analysis. Induced internal gradients caused by the magnetic susceptibility contrast within a system are known to create additional relaxation of transverse magnetization because of the dephasing of spin coherence.

We focus on the relaxation in inhomogeneous field that are induced by paramagnetic particles in water-saturated pores, with simple cylindrical structure (Zhang et al., 2003).

In this space, de Swiet and Sen (1994); Hürlimann (1998); Anand and Hirasaki (2008) defined three relevant length scales:

1. Diffusion length, $L_d(\text{micrometers}) = \sqrt{D\tau_{E,}}$ (10)

   where τ_E is half the t_E used in the CPMG pulse sequence and D is the diffusivity of the fluid

2. Pore structural length (micrometers), L_s, and

3. Dephasing length, $L_g(\text{icrometersm}) = \sqrt[3]{\frac{D}{\gamma G}}$ (11)

The smallest length-scale determines which of the three possible relaxation regimes (motional averaging, which is characterized by fast diffusion of protons such that the nuclear spin interaction caused by inhomogeneities in magnetic field are motionally average, free diffusion and localization), will dominant secular relaxation in a constant gradient. Similarly, Gillis and Koenig (1987), Brooks et al. (2001), Gillis et al. (2002), Anand and Hirasaki (2008) considered the equivalent of these three regimes in inhomogeneous fields as *motional averaging*, *weak magnetization and strong magnetization*, based on the dominant of these three characteristic time scales:

1. $\tau_E = \frac{t_E}{2}$ (12)

2. $\tau_\omega = \frac{1}{\delta\omega} = \frac{(k+1)}{3(k-1)\gamma B_0}$ (13)

   (time taken for substantial dephasing, τ_ω and expressed as the inverse of the spread in Larmor frequency [$\delta\omega$ in radians/second] in the system and

   $k = (1 + \chi_{\text{grains}})/(1 + \chi_{\text{fluid}})$. (14)

   The Larmor frequency, ω (radians per seconds), is the frequency at which magnetic moment precess around applied field, (Levitt, 2008).

3. $\tau_R = \frac{L^2}{D}$ (15)

(τ_R is the diffusional correlation time, expressed as the time taken to diffusionally average the inhomogeneities and L is the length of variation of the magnetic field in the system).

These time scales will characterize secular relaxation in inhomogeneous fields, into relaxation regimes as follows (Gillis and Koenig, 1987; Jensen and Chandra, 2000; Brooks et al., 2001; Gillis et al., 2002; Anand and Hirasaki, 2008):

I. Motional averaging regime: Here, inhomogeneities in magnetic field are motionally averaged because of fast diffusion of protons. Its governing conditions are defined as $\tau_R \ll \tau_\omega$ and $\tau_R \ll \tau_E$; and $\frac{1}{T_{2,sec}} = \frac{16}{405}\Phi\delta\omega^2\tau_R (\Phi = \frac{\text{mass (dry sample)}}{\text{mass (dry+brine) after compaction}}$ (16)

is the volume fraction of the paramagnetic particles and it is dimensionless).

II. Free diffusion regime (weak magnetization regime). Here spins dephase as if diffusing in a medium unaffected by large field inhomogeneities or restriction. The defining conditions are $\tau_E \ll \tau_\omega$ and $\tau_E \ll \tau_R$; and $\frac{1}{T_{2,sec}} = \frac{\delta\omega^2\tau_{E^2}}{5\tau_R}$. (17)

III. Localization regime (strong magnetization regime). In this situation, relaxation is in presence of superparamagnetic particles with strongly magnetized contrast agents $\tau_\omega \ll \tau_R$ and$\tau_\omega \ll \tau_E$; and $\frac{1}{T_{2,sec}} = \frac{\delta\omega^2\tau_{E^2}}{5\tau_R}\left(\frac{\delta\omega\tau_E}{a+b\Phi\delta\omega\tau_E}\right)^{-\frac{5}{3}}$ (18)

(parameter values: a = 4.5 and b = 0.99).

Further characterizing secular relaxation theory in terms of dimensionless quantities, which is unaffected by particular system parameter, is given by Anand and Hirasaki (2008):

$$\frac{1}{T_{2,sec}^{D}} = t_0 \frac{1}{T_{2,sec}} \quad (19)$$

where $1/T_{2,sec}^{D}$ is the simulated dimensionless relaxation rate and $t_0 = 3/\Phi\delta\omega$ is a characteristic time (seconds).

2.2.6 Pore size distribution, Bound Fluid Volume (BFV) and Permeability

In general, small pores shorten T_2 relaxation and correspond to clay bound and capillary bound water (*BFV*), and separated by a cutoff ($T_{2\text{cutoff}}$) from large pores, which allow long T_2 relaxation and host producible fluids (Kenyon et al., 1995). Thus, relaxation time distribution is a measure of pore size distribution. Brownstein and Tarr (1979) classified pore sizes for a "fast diffusion" regime, indicating that relaxation rate is directly proportional to surface-to-volume ratio; for a "slow diffusion" regime, it is inversely proportional to the square of the pore size. In this research, we applied the classification by Hürlimann (1998) to differentiate between small and large pore subsets. Small pores are less than L_g but large pores will be larger than L_g. This classification estimates that the dephasing echo is governed by free diffusion in large pores and the Larmor Frequency value may encounter less uncertainty or spread whereas internal field inhomogeneities are motionally averaged in small pores. The expression for the apparent pore size classification is therefore given by

$$l^a = \left(\frac{D}{\gamma B_0 \Delta\chi}\right)^{1/2} \quad (20)$$

We also assumed the pore structure for samples investigated to be cylindrical and calculated the average pore radius from: $r \; or \; R = 2\left(\frac{Volume}{Surface}\right) = \left(\frac{2}{Spor}\right)$ (21)

(Zhang et al., 2001). We expect field inhomogeneities to exist over the entire length (diameter) of the pore (Callaghan, 1995; Anand, 2007), so that the length of variation of field inhomogeneity in the system is, $L = 2R$. In this report, we present indices that will identify the anomalies encountered when determining T_{2ML}^{-1} or $T_{2\text{cutoff}}$, the primary inputs into the two established permeability equations (SDR or Timur-Coates).

2.3 MATERIALS AND METHODS

2.3.1 Sample Preparation and Characterization

The eight samples used in this study are all natural samples acquired from three mineral repository establishments. Most samples were either received as powder (particle size < 38 μm or 1.25 x 10^{-4} ft.) whereas the bulky ones were crushed and/or sieved using 300μm (1.0 x 10^{-3} ft.) size mesh. Illite, glauconite, and pyrite were sourced from Wards Scientific; celadonite and chamosite were acquired from Excalibur Mineral Corporation; montmorillonite and kaolinite were obtained from Source Clays Repository. These minerals are shale-prone aggregates that can occur in diverse combinations. The mineralogy for all samples was verified using X-Ray diffraction (XRD; Bruker D8 Advance X-Ray Diffractometer), and elemental analysis was performed using X-ray fluorescence (XRF; Thermo Scientific X-Ray Fluorescence). To determine the volumetric magnetic susceptibility (MS), dry samples were packed into 20 cm^3 (1.2 $in.^3$) cylindrical bottles, and measured at a low frequency of 0.465 kHz (Bartington MS2 Magnetic Susceptibility System). The specific surface area S_s, defined as the surface area

normalized by the sample mass, was measured using the Brunauer-Emmett-Teller gas adsorption method with nitrogen gas N_2 (g) as the adsorbate, for example in Lowell and Shield (2013) (ASAP 2020; Micromeritic Instrument Corp). A 125 g/L NaCl brine was used to saturate all samples. NMR samples were made by creating a mineral-brine slurry and then centrifuging to compact the solid phase and decanting the fluid phase. All slurries were prepared using a mineral-to-brine ratio of 1:2 by mass except for celadonite, which was prepared using a ratio of 1:3 because of the quantity of celadonite available. Slurries were compacted by centrifuging at 600 psi (4.14×10^6 Pa) (Eppendorf Centrifuge 5804) and residual air bubbles were removed at intervals during compaction with Vortex-2 Gene.

2.3.2 NMR Measurement Procedure

NMR relaxation data were collected with 2-MHz Magritek Rock Core Analyzer using a CPMG (Carr- Purcell-Meiboom-Gill) pulse sequence. Data for each sample were collected at 10 echo times: 150, 200, 300, 400, 500, 600 800, 1000, 1200, 1500 μs, with delay time stacks being at least three times the relaxation time. The number of echoes collected was 30 for celadonite, 40 for montmorillonite, 50 chamosite and illite, 60 for glauconite, 150 for pyrite and 200 for kaolinite. Each measured magnetization decay signal for a T_2 distribution was inverted using a regularized nonnegative least squares algorithm after Whittall et al. (1991). In this method, the data were fitted to a distribution of 160 logarithmically spaced T_2 values, from 10^{-4} to 10^{1} s and then the inverted model was regularized for smoothness, which limits inversion artifacts. A single value, the mean

log relaxation time, T_{2ML}, was used to represent the NMR relaxation behavior of the samples and it is expressed as the sum of three relaxation rates (T_2: bulk, surface and diffusion). Separate repeat measurements were conducted for each sample to determine experimental error. Longitudinal T_1 measurement for each sample was performed using inversion recovery sequence. The S_{por} was determined using equation according to Keating and Knight (2010). T_1-T_2 measurement was performed on all the samples according to Song et al. (2002), at 2 MHz proton resonance frequency. $^{\tau_1}/_{\tau_2}$ (22) varied logarithmically from a minimum of 0.2 ms to maximum of 1 s. Here, τ_1 refers to the time period over which the spin magnetization decays along the z axis and during τ_2, the decay is caused by T_2. To improve the signal-to-noise ratio, data was stacked 256 times, and the signal-to-noise ratio set to 200 for all T_1, T_2, and T_1-T_2 measurements. All measurements were made at 30°C to avoid changes in the NMR response because of variations in temperature.

2.4 DATA AND RESULTS

2.4.1 Physical Properties

This study reviewed the bias that can be introduced because of internal magnetic field gradients created by constituent minerals, when classifying the pore-size distribution in shale. The weight percentages of Fe and Mn in each of the samples, measured with XRF elemental analysis, are presented along with elements in Table 2-1.Total iron concentrations in the samples measured from 0.3% in kaolinite, to approximately 42% in

pyrite. The manganese concentration was undetected in most samples except in illite, chamosite and glauconite, which measured approximately 0.05%, 0.5% and 0.1% respectively. As basic quality assurance measure, the weight percentages of Fe and Mn were determined to be consistent with what is reported in literature (Carmichael, 1982; Dearing, 1994; Dodge et al., 1995; Matteson et al., 1998; G. Q. Zhang et al., 1998; Keating and Knight, 2010) The XRD results confirmed the mineralogy of all the samples except for celadonite, which was observed to contain minor inclusion of glauconite.

The T_2 relaxation rate of pore fluids for any given iron mineral would be proportional to the concentration of iron on the solid phase of the pore surface (Foley et. al., 1996; Bryar et. al., 2000). G. Q. Zhang et al (1998) demonstrated in experiments that iron-rich clays with high magnetic susceptibility induce strong internal field gradients and shorten the T_2 in a system. The volume magnetic susceptibility values for the samples are listed in Table 1-1. These values range from -9 X 10^{-6} (Hürlimann, 1998) to 438 X 10^{-6} Standard International [SI] units. Whereas pyrite has the highest iron concentration (42 wt. %), it is chamosite that contains the most manganese (0.5 weight percent), measuring the highest magnetic susceptibility at 438 X 10^{-6} [SI]. However, all the samples recorded positive magnetic susceptibility values except kaolinite (Table 1-1). The values of S_s for each mineral sample ranged from 0.1 for pyrite to 91.5 m^2/g for montmorillonite (Table 1-1). Montmorillonite with the same grain size as kaolinite (<38 μm or 1.25 x 10^{-4} ft.), has the highest S_s (91.5 m^2/g) and although glauconite, celadonite and illite have bigger grain size (<300 μm or 1.0 x 10^{-3} ft.) than kaolinite, they all have higher S_s at 53.0, 33.0 and 19.0 m^2/g respectively, compared to kaolinite at 12.0 m^2/g (Table 2-1).

Table 2-1. Chemical and Physical Properties of Brine and Mineral Samples

Material Name	Iron, (wt.%)	Manganese, (wt.%)	MS (x 10^{-6} SI) ($\Delta\chi$)	Specific Surface Area, (m^2/g)	Grain Sizes, (μm)
Brine	-	-	-9.1	-	-
Kaolinite	0.3	0	-5.0	12.0	< 38
Montmorillonite	1.5	0	8.0	91.5	< 38
Glauconite	23.5	0.1	57.0	53.0	< 300
Pyrite	42.0	0	91.0	0.1	< 300
Illite	7.0	0.05	217.0	19.0	< 300
Celadonite	20.5	0	225.0	33.0	< 300
Chamosite	21.0	0.5	438.0	2.0	< 300

Abbreviations: — = not applicable; $\Delta\chi$ = magnetic susceptibility contrast between the pore fluid and grain matrix; MS = magnetic susceptibility; SI = standard international units.

2.4.2 Nuclear Magnetic Resonance Relaxation

The relaxation time distribution measured at 10 t_E (150 – 1500 μs) was used to calculate T_{2ML} for each mineral/brine mixture compacted at 600 psi (4.14 x 10^6 Pa). The T_{2ML} values used in this analysis were from long and short t_E as well as computed average T_{2ML} values. Note that only a single T_2 distribution peak was observed for each sample slurry. In decreasing order of average relaxation times, celadonite had the longest relaxation time; montmorillonite, kaolinite and pyrite peak positions were similar with their shorter relaxation times, whereas glauconite chamosite and illite measured the shortest relaxation times. The T_{2ML} value at long t_E relaxed faster than the average, which relaxed faster than at short t_E for glauconite, illite, kaolinite and pyrite. The T_{2ML} value at short t_E relaxed faster than the average, which relaxed faster than the long t_E for chamosite and montmorillonite. The T_{2ML} at short t_E relaxed faster than the T_{2ML} at long t_E, which was faster than the average T_{2ML} for celadonite. Although the pore size remained unchanged, the value of $V_w$at the short t_E was larger than the average, and the average V_w value was greater than at long t_E for montmorillonite, pyrite, illite, celadonite and chamosite. The V_w value at long t_E was larger than the average which was larger than the V_w at short t_E for kaolinite. Observed variations in the values of V_w and T_{2ML} for long and short t_E, in unchanged pore system may indicate paramagnetism effects on the measurement.

The T_1/T_2 map above the dashed 1:1 line in Figures 2-1 (A-F) indicates that relaxation in the pores might have occurred in the presence of an induced internal magnetic gradient. The small deviations away from the 1:1 line (for montmorillonite,

glauconite and illite) are caused by noise and the limitations imposed by the inversion algorithm. Inhomogeneities in the magnetic field result in diffusion relaxation, which speeds up relaxation and is a function of the t_E (Song et al., 2002). For montmorillonite, glauconite and illite sample, T_1/T_2 maps plotted slightly above the 1:1 line (Figures 2-1A, D and E) but chamosite, pyrite and kaolinite (Figures 2-1B, C and F) plotted well above the 1.1 (unity) line. This suggests presence of marginal magnetic field inhomogeneities for the previous and strong magnetic field inhomogeneities for the latter samples. Celadonite plotted on the 1:1 (unity) line (Figure 2-1G). The T_1/T_2 ratio of unity for celadonite indicates a weak or absent magnetic field inhomogeneity effect on T_2 relaxation.

To comprehend the magnitude of internal gradients on diffusion relaxation rate, the dependence of T_{2ML}^{-1} on t_E was determined. Overall yield of positive slope from a plot of T_{2ML}^{-1} versus the square of the t_E (t_E^2) will indicate presence of internal gradient (i.e. $G \neq 0$). The T_{2ML}^{-1} linearly increased with t_E^2 for small t_E for at least the first two t_E with all the samples except in montmorillonite (Figure 2-2). The general trend for celadonite and montmorillonite was negative

and this agrees with the plot of their T_1/T_2 ratio. Kaolinite, which has a low magnetic susceptibility value, showed a weak but consistently positive slope. In general, the slope of glauconite, illite, and positive all showed positive trends. Chamosite T_{2ML}^{-1} values decreased for the last five t_E measured. Based on the outcome of these plots, it is reasonable to expect that montmorillonite, celadonite or the last five echo spacing data from chamosite, which encounters weak dependence of relaxation rate on t_E, may average out the internal gradient effects on their T_2 relaxation.

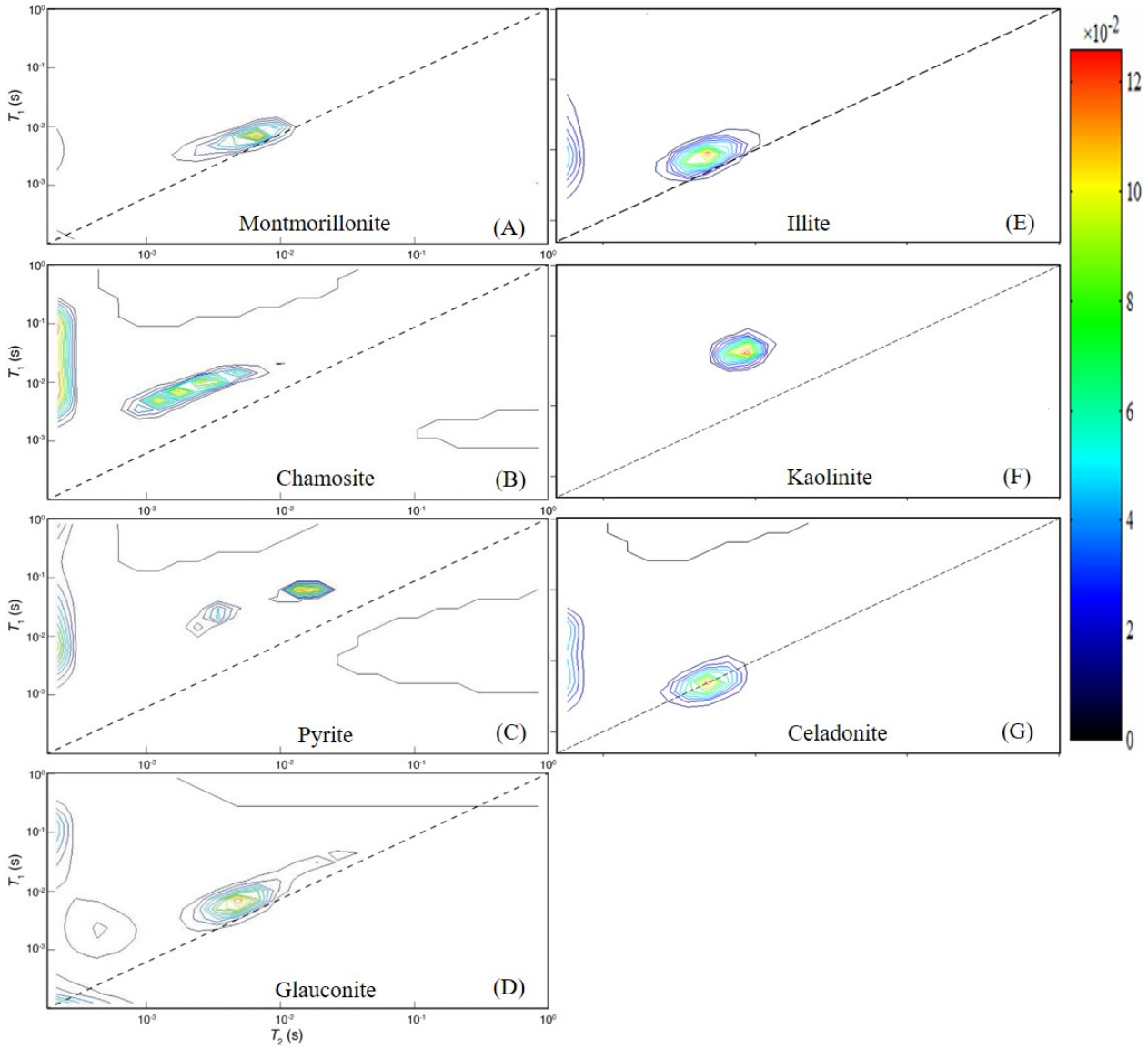

Figure 2-1. (A-G): Longitudinal relaxation time to transverse relaxation time (T_1/T_2) correlation maps for mineral slurries. Points above the dashed line are positive and indicate the presence of magnetic field inhomogeneity. Maps for chamosite, kaolinite and pyrite are distinctly above the unity line. Montmorillonite and glauconite slurries plot close to the unity line. Celadonite plotted on the unity line. The T_1/T_2 ratio increases with the paramagnetic particle size (Anand, 2007). Dashed line is 1:1 (unity).

Samples were fit into different relaxation regimes based on their computed characteristic time scales and they indicate that relaxation of all the mineral slurries occurred in the localization regime except celadonite and montmorillonite, which fit into the motional averaging regime. In addition, as observed from the T_{2ML} dependence t_E data, at long t_E (1500 μs) the relaxation of chamosite changed from the localization to the motional averaging relaxation regime (Table 2-2). Pore size distribution was computed from the average NMR data of the samples based on the model by Hürlimann (1998). The model expects that large pores will be governed by free diffusion whereas small pores are motionally averaged. Both montmorillonite and celadonite fit the large pore criteria but all the other samples matched the small pore criteria at long/short t_E and average data. The internal gradient $\boldsymbol{G_{max}}$ is larger in montmorillonite and celadonite than in all other slurry (Table 2-3). Although kaolinite relaxation occurred in the localization regime, it had the least measured internal gradient at 411 gauss/cm.

The magnetic susceptibility contrast Δχ, between the matrix and the fluids all recorded positive values. High magnetic susceptibility induces strong internal field gradients in systems such as clays that contain iron-rich materials, and shorten the T_2 relaxation (G. Q. Zhang et al., 1998). In all the measurements, the internal gradient in the slurries dominated the tool gradient (external gradient) in the Magritek analyzer.

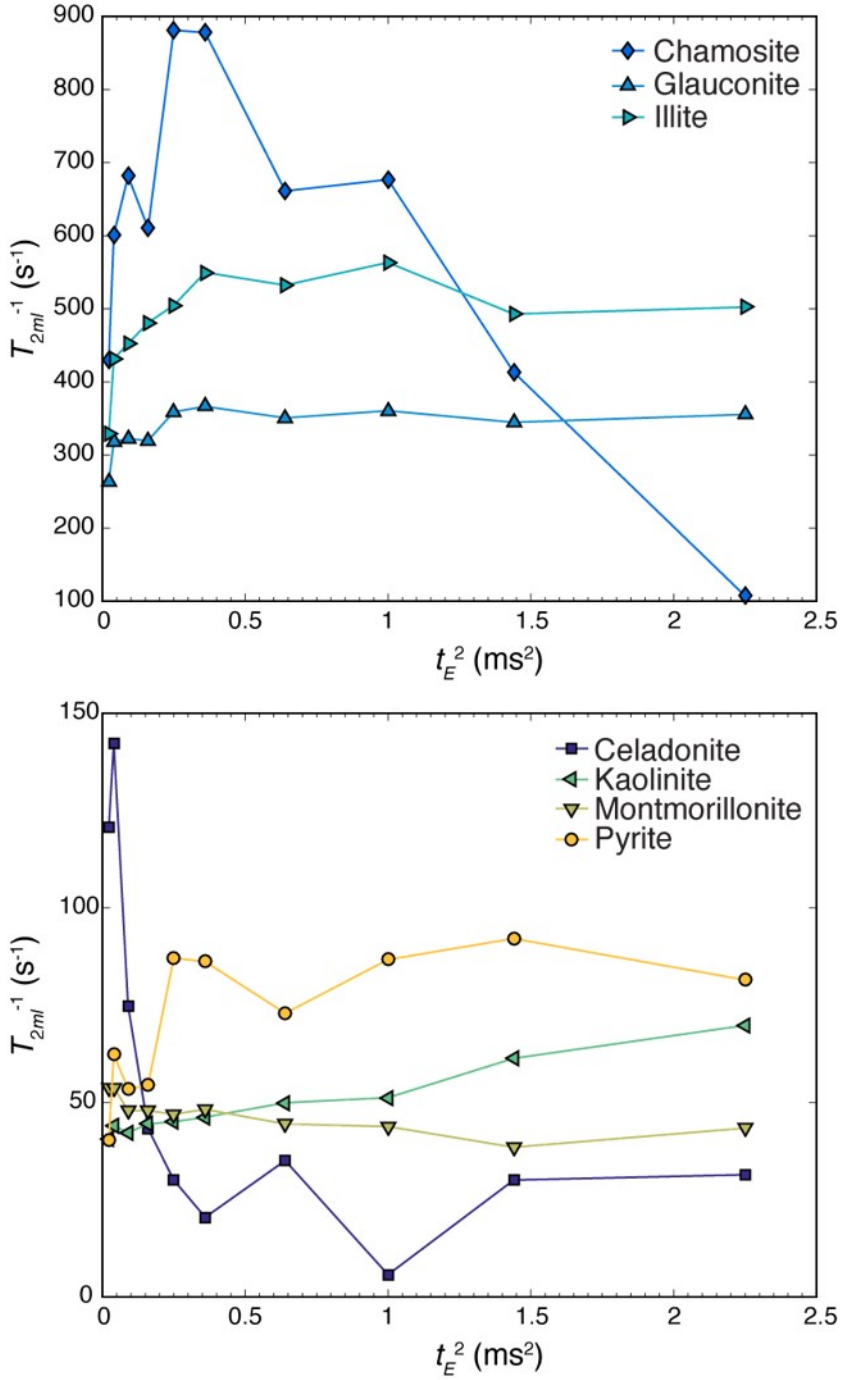

Figure 2-2 (A-B): Plot of $1/T_{2ML}$ (total mean logarithm transverse relaxation time) versus t_E^2 (square of t_E) showing the dependence of transverse relaxation time (T_2 in seconds) on echo spacing (t_E in milliseconds). **(A)** Show plot of chamosite, glauconite and illite **(B)** Show celadonite, kaolinite, montmorillonite and pyrite.

2.5 DISCUSSIONS

Our initial inquiry focused on establishing the presence and magnitude of internal gradients on NMR relaxation of the samples. The magnitude of the computed internal gradients in the slurries dominated the external (tool) gradients from the NMR analyzer. We expected that the amount of iron in the minerals and the $\Delta\chi$ values in the slurries would control the magnitude of internal gradients but no reasonable correlation was observed between these parameters. The T_2 relaxation rate of the minerals can be affected by the presences of internal magnetic field gradients and the shortest time scales reflect their characteristics. These characteristic times will also determine the behavior of the relaxation regimes such as T_1/T_2 ratio and dependence on t_E (Anand and Hirasaki, 2008). The T_2 relaxation of pyrite, glauconite, illite, and kaolinite was determined to have occurred in the localization regime because the time taken for significant dephasing τ_ω, was the shortest time scale ($\tau_\omega << \tau_R$ and $\tau_\omega << \tau_E$) (Table 2-2). This regime indicates a situation with strongly magnetized contrast between particles and the medium, such as exists with superparamagnetic materials ($\delta\omega\tau_E > 1$). For these minerals, the dependence of the relaxation rate on the t_E and their T_1/T_2 ratio were both slightly to strongly positive (Figure 2-1, 2-2). The behavior of chamosite was a bit peculiar because it was governed by localization regime in the shorter t_E, and dominated by motional averaging regime in the longer t_E. Chamosite T_1/T_2 ratio was distinctly positive and the shorter t_E indicated dependence of the relaxation rate on t_E whereas the longer t_E did not show such dependence. The T_2 relaxation of montmorillonite and celadonite also occurred in the

motional averaging regime, because their shortest time scale was the diffusional correlation time τ_R, ($\tau_R << \tau_E$ and $\tau_R << \tau_\omega$). Both samples had the largest internal gradients yet showed no dependence of the relaxation rate on the t_E and their T_1/T_2 ratio was on or near the unity line (Figure 2-1, 2-2).

Table 2-2. Characteristic Time Scales for Average Echo Spacing Data and Long Echo Spacing and Relaxation Regimes of Samples

	Time scale (ms)			
Material Name	τ_E	τ_ω	τ_R	**Relaxation Regime**
Kaolinite	75	<0	3	Localization
Montmorillonite	75	0.01	0.003	Motional Averaging
Glauconite	75	0.13	0.2	Localization
Pyrite	75	0.13	1800	Localization
Illite	75	0.15	0.8	Localization
Celadonite	75	0.16	0.004	Motional Averaging
Chamosite	75	0.16	13	Localization
Chamosite (Long t_E)	750	0.16	0.011	Motional Averaging

Abbreviations: τ_ω = time taken for substantial dephasing; τ_E = half the echo spacing used in the Carr–Purcell–Meiboom–Gill pulse sequence; τ_R = the diffusional correlation time; t_E = echo spacing.

Although the calculated pore size remained unchanged, in glauconite, pyrite, illite, celadonite, montmorillonite and chamosite, the internal gradients was higher at long t_E than at short t_E but reverse in kaolinite (Table 2-4). In addition, T_{2ML} shortened for all the minerals except montmorillonite, chamosite and celadonite (Figure 2-3). Based on the criteria put forth in Hürlimann (1998), celadonite and montmorillonite pore systems were

computed as large pores but rather than being governed by the free diffusion as proposed, we determined that their relaxation was in the motional averaging regime. Similarly, the computed pore sizes of the rest of the samples were small pore systems and again contrary to the Hürlimann (1998) criteria, the internal field inhomogeneities were not all motionally averaged in these small pores, rather they were dominated by the localization regime. However, the long t_E chamosite had relaxation in the motional-averaging regime and no dependence on t_E (Table 2-2).

Table 2-3. Maximal Effective Internal Magnetic Field Gradient, Dephasing Length, l^a, and Pore Sizes of Average Echo Spacing Data of the Samples

Material Name	G_{max} at 2 MHz, (gauss/cm)	L_g, (µm)	l^a, (µm)	Pore Size
Kaolinite	411	0.0240	0.0180	Small
Montmorillonite	56,980	0.0050	0.0085	Large
Glauconite	42,370	0.0050	0.0043	Small
Pyrite	447	0.0230	0.0035	Small
Illite	49,210	0.0050	0.0023	Small
Celadonite	748,260	0.0020	0.0023	Large
Chamosite	23,642	0.006	0.0017	Small

Abbreviations: l^a = apparent size for classifying large and small pores; G_{max} = maximal effective internal magnetic field gradient; L_g = dephasing length.

So far, some aspects of our interpretation, and the classification of their relaxation regimes did not seem congruent with the physical properties of some of the samples. For

example, the computed data for kaolinite indicated relaxation in the localization regime. However, the kaolinite used in this study was diamagnetic with negligible iron concentrations and very low $\Delta\chi$ value, and expected to have less diffusion effects (G. Q. Zhang et al., 1998). Hence, we generated dimensionless relaxation rates ($1/T_{2,sec}^{D}$) as a function of normalized diffusion correlation time ($\delta\omega\tau_R$) and normalized t_E ($\delta\omega\tau_E$) parameters according to Anand and Hirasaki (2008) (Figure 2-4). The outcome of the dimensionless quantities validated the secular relaxation regime for all the samples. It indicated that kaolinite is essentially governed by the free diffusion regime ($\delta\omega\tau_E << 1$ and $\delta\omega\tau_E << \delta\omega\tau_R$) whereas there was no change in rest of the classifications. Montmorillonite, celadonite and long t_E chamosite were still governed by the motional averaging regime ($\delta\omega\tau_E >> 1$ and $\delta\omega\tau_R << 1$), and all other minerals still dominated by the localization regime ($\delta\omega\tau_E >> 1$ and $\delta\omega\tau_R >> 1$). Additionally, the effects of internal gradient on the samples were evidenced by increased $1/T_{2,sec}^{D}$ from the short to long t_E for all the samples except kaolinite, which showed negligible rate (Figure 2-5).

Table 2-4. The Internal Gradient at Short and Long Echo Spacing, Pore Size, and Total Mean Logarithm of Transverse Time Relaxation

Material Name	gG_{max} at 2 MHz, gauss/cm	l^a, µm	T_{2ML}
Kaolinite (S)	430	0.0180	0.0250
Kaolinite (L)	370	0.0180	0.0140
Montmorillonite (S)	45,310	0.0085	0.0200
Montmorillonite (L)	66450	0.0085	0.0230
Glauconite (S)	43,190	0.0043	0.0040
Glauconite (L)	49,330	0.0043	0.0030
Pyrite (S)	438	0.0035	0.0250
Pyrite (L)	530	0.0035	0.0120
Illite (S)	45,850	0.0023	0.0030
Illite (L)	78,550	0.0023	0.0020
Celadonite (S)	251,070	0.0023	0.0080
Celadonite (L)	237,264,000	0.0023	0.0320
Chamosite (S)	16,603	0.0017	0.0023
Chamosite (L)	794,944	0.0017	0.0093

Abbreviations: l^a = apparent size for classifying large and small pores; G_{max} = maximal effective internal magnetic field gradient; L = long; S = short; T_{2ML} = total mean logarithm of transverse relaxation time.

We observed that the volume fraction Φ, for celadonite and montmorillonite both in the motional averaging regime was ≤ 0.6 whereas the value was greater for the rest of the minerals. In addition, we expected celadonite with high iron content and high magnetic susceptibility value to be dominated by the localization regime but the low Φ value may have contributed to its internal field inhomogeneities being motionally averaging (Figure 2-4). Surface concentrations of paramagnetic species are directly

proportional to the relaxivity and low surface concentrations show no relaxation dependence on t_E (Foley et al., 1996; Anand and Hirasaki, 2008; Washburn, 2014).

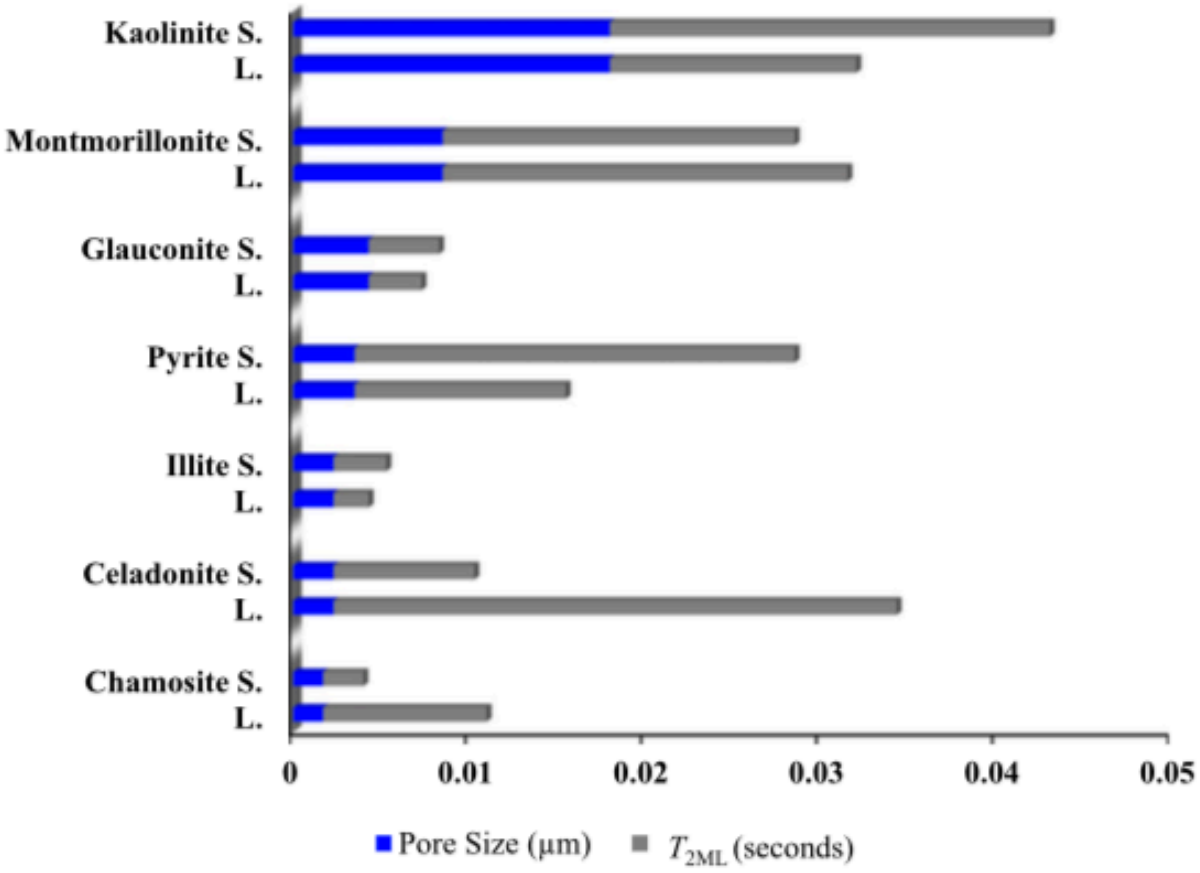

Figure 2-3. Stacked bar graph of computed pore size (blue bar in micrometers) and the total mean logarithm of transverse relaxation time (T_{2ML}; gray bar). The internal gradient increased from the short (S.) to long (L.) echo spacing (t_E, in milliseconds) in all of the samples except in kaolinite.

Finally, the value of the secular relaxation rate may be the difference between the measured and the actual T_2 relaxation rate caused by magnetic field inhomogeneities in a

porous media. This rate as determined in this research will influence the relaxation regimes of the pore and create error in the pore size distribution and classification of *BFV*. This effect occurs because of molecular diffusion in inhomogeneous fields. Although running CPMG pulse sequence with the shortest possible t_E at low fields such as the 2-MHz analyzer used in this research can mitigate diffusion effects (Kleinberg and Vinegar, 1996; Hürlimann, 1998), the impact of the effects was observed to manifest as shortened relaxation time even at short range of t_E. The extra relaxation time removed from T_{2ML} consequently, may result in the overestimation of *BFV* and when used as input into any of the two permeability estimators (Timur-Coates or SDR) will result in the underestimation of permeability.

2.6 CONCLUSIONS

We set out first to determine presence and magnitude of internal gradients in shale by considering the effect on constituent minerals. Minerals with high iron content and the magnetic susceptibility will induce strong internal field gradients and shorten the T_2 inside a pore space. The T_1/T_2 ratio and dependence of relaxation rate on t_E were applied in this study to validate the presence and magnitude of the internal gradients in brine/minerals slurry. Based on the models put forward by Kleinberg and Vinegar (1996), G. Q. Zhang et al. (1998, 2003), Hürlimann (1998), and Anand and Hirasaki (2008), we defined the pore geometry and magnitude of the internal gradients, characterized the pore size distributions, and categorized the secular relaxation regimes. The computed internal gradient was the dominant gradient and all of the minerals were computed as having

small pore except celadonite and montmorillonite. In addition, kaolinite was governed by free diffusion regime; montmorillonite, celadonite and long t_E chamosite were dominated by motional averaging regime whereas localization regime dominated the relaxation of illite, glauconite, pyrite and short t_E chamosite. The implication of these classifications is that T_{2ML} shifts to faster time, resulting in the overestimation of BFV, which when used as input parameter into permeability equation, will lead to underestimation of NMR permeability.

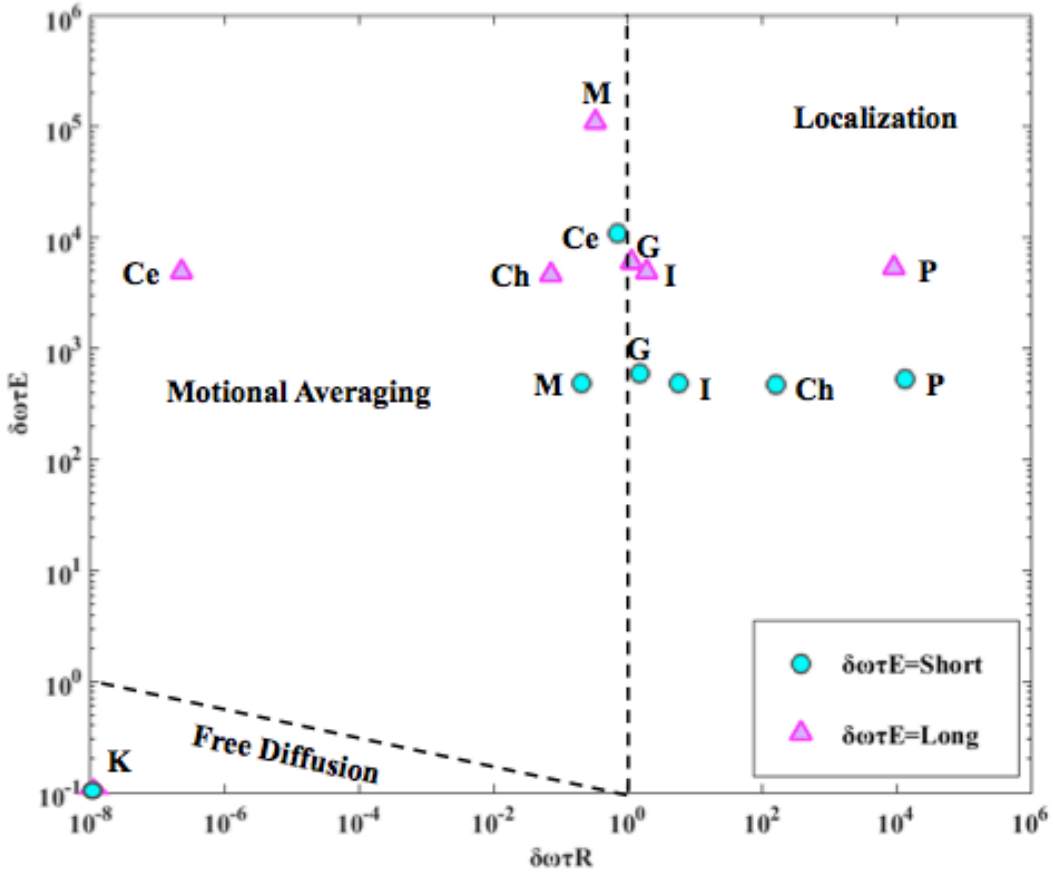

Figure 2-4. Plot showing the classification of minerals under their dominant relaxation regimes based on two dimensionless parameters: normalized echo spacing ($\delta\omega\tau_E$) and normalized diffusional correlation time $\delta\omega\tau_R$. The boundaries that delineate the regimes are represented by the dashed lines, $\delta\omega\tau_E = 1$ and $\delta\omega\tau_R = 1$. Ce = celadonite; Ch = chamosite; G = glauconite; I = illite; K = kaolinite; M = montmorillonite; P = pyrite.

We conclude that internal gradients, although induced by paramagnetic and clay minerals common in shale, will vary with t_E, and the concentration or volume fraction of the paramagnetic particles in a porous media. Although the results of our study underscores the need to modify the approach of petrophysical interpretation of shale

reservoirs using transverse T_2 relaxation time, it is not expected to serve as a definitive guide. Further experimental and simulation work are required because of the wide range of heterogeneities associated with shale.

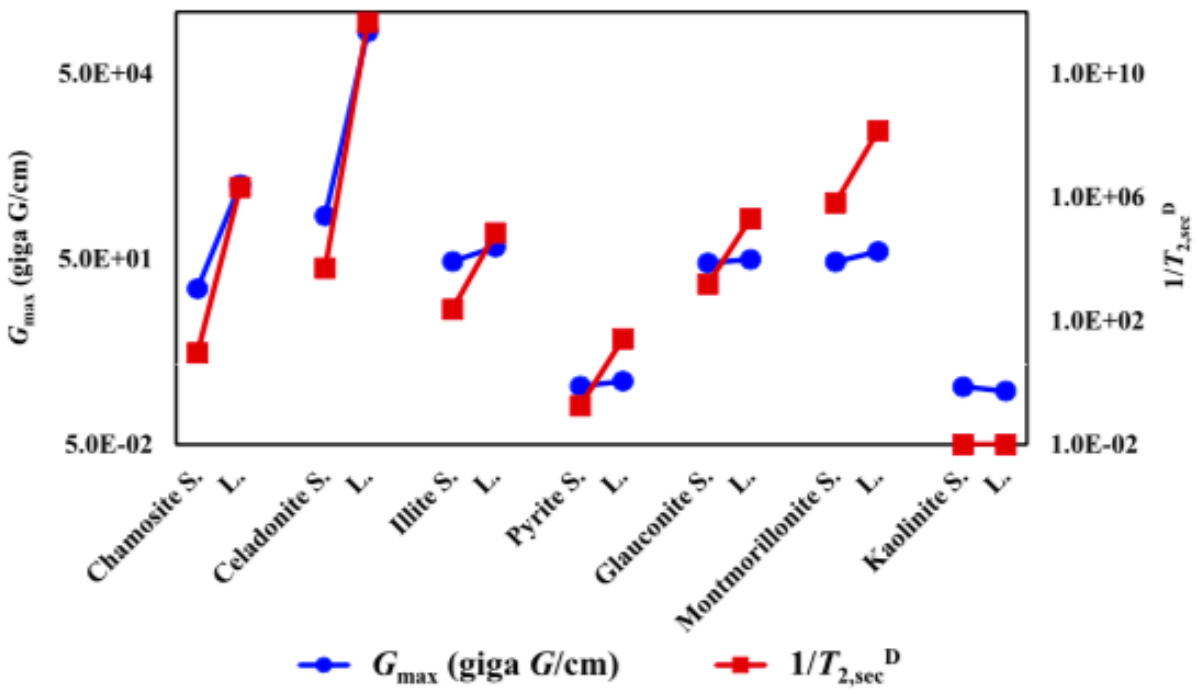

Figure 2-5. Plot of maximal effective internal magnetic field gradient (G_{max}; blue line, in gauss per centimeter [G/cm]) and normalized secular simulated dimensionless relaxation rate ($1/T_{2,sec}^{D}$; red line). Negligible values for kaolinite at long (L.), short (S.) echo spacing (t_E, in milliseconds).

REFERENCES CITED

Akkurt, R., H. J. Vinegar, P. N. Tutunjian, and A. J. Guillory, 1995, NMR logging of natural gas reservoirs: Society of Petrophysicists and Well Log Analysts (SPWLA) 36th Annual Logging Symposium, Paris, France, June 26–29, 1995, SPWLA-1996-v37n6a1, 12 p.

Allen, D. F., A. Boyd, J. Massey, E. J. Fordham, M. O. Amabeoku, W. E. Kenyon, and W. B. Ward, 2001, The practical application of NMR logging in carbonates: 3 case studies: Society of Petrophysicists and Well Log Analysts (SPWLA) 42nd Annual Logging Symposium, Houston, Texas, June 17–20, 2001, SPWLA-2001-K, 14 p.

Anand, V., 2007, NMR oil well logging: diffusional coupling and internal gradients in porous media, Ph.D. thesis, Rice University, Houston, Texas, 206 p.

Anand, V., and G. J. Hirasaki, 2008, Paramagnetic relaxation in sandstones:

Distinguishing T 1 and T 2 dependence on surface relaxation, internal gradients and dependence on echo spacing: Journal of Magnetic Resonance, v. 190, no. 1, p. 68–85, doi:10.1016/j.jmr.2007.09.019.

Bachman, H., S. F. Crary, R. Heidler, J. A. La Vigne, and R. Akkurt, 2007, Porosity determination from NMR log data: The effects of acquisition parameters, noise, and inversion: Society of Petroleum Engineers (SPE) Annual Technical Conference and Exhibition, Anaheim, California, November 11–14, 2007, SPE-110803-MS, 11 p., doi: 10.2118/110803-MS.

Bloembergen, N., E. M. Purcell, and R. V. Pound, 1948, Relaxation effects in nuclear magnetic resonance absorption: Physical Review, v. 73, no. 7, p. 679–712, doi: 10.1103/PhysRev.73.679.

Brooks, R. A., F. Moiny, and P. Gillis, 2001, On T_2-shortening by weakly magnetized particles: The chemical exchange model: Magnetic Resonance in Medicine, v. 45, no. 6, p. 1014–1020, doi:10.1002/mrm.1135.

Brownstein, K. R., and C. Tarr, 1979, Importance of classical diffusion in NMR studies of water in biological cells: Physical Review A, v. 19, no. 6, p. 2446–2453, doi: 10.1103/PhysRevA.19.2446.

Bryar, T. R., C. J. Daughney, and R. J. Knight, 2000, Para- magnetic effects of iron (III) species on nuclear magnetic relaxation of fluid protons in porous media: Journal of Magnetic Resonance, v. 142, p. 74–85.

Callaghan, P. T., 1995, Pulsed-gradient spin-echo NMR for planar, cylindrical, and spherical pores under conditions of wall relaxation: Journal of Magnetic Resonance. Series A., v. 113, no. 1, p. 53–59, doi:10.1006/jmra.1995.1055.

Carmichael, R. S., ed., 1982, CRC handbook of physical properties of rocks: Boca Raton, Florida, CRC Press, v. 2, 360 p.

Carr, H. Y., and E. M. Purcell, 1954, Effects of diffusion on free precession in nuclear

magnetic resonance experiments: Physical Review, v. 94, no. 3, p. 630–638, doi: 10.1103/PhysRev.94.630.

Chen, S., R. Arro, C. Minetto, D. Georgi, and C. Liu, 1998, Methods for computing SWI and BVI from NMR logs: Society of Petrophysicists and Well Log Analysts (SPWLA) 39th Annual Logging Symposium, Keystone, Colorado, May 26–28, 1998, SPWLA-1998-HH, 10 p.

Coates, G. R., and J. L. Dumanoir, 1973, A new approach to improved log-derived permeability: Society of Petro- physicists and Well Log Analysts (SPWLA) 14th Annual Logging Symposium, Lafayette, Louisiana, May 6–9, 1973, SPWLA-1973-R, 28 p.

Coates, G. R., D. Marschall, D. Mardon, and J. Galford, 1998, A new characterization of bulk-volume irreducible using magnetic resonance: Log Analyst, v. 39, p. 51–63.

Coates, G. R., L. Xiao, and M. G. Prammer, 1999, NMR logging: Principles and applications: Houston, Texas, Haliburton Energy Services, 251 p.

Cornell, R. M., and U. Schwertmann, 2003, The iron oxides: Structure, properties, reactions, occurrences and uses, 2nd ed.: Hoboken, New Jersey, Wiley-VCH, 137 p., doi:10.1002/3527602097.

Costabel, S., and U. Yaramanci, 2013, Estimation of water retention parameters from nuclear magnetic resonance relaxation time distributions: Water Resources Research, v. 49, no. 4, p. 2068–2079, doi:10.1002/wrcr.20207.

Dearing, J., 1994, Environmental magnetic susceptibility: Using the Bartington MS2 system: Kenilworth, United Kingdom, Chi Publishing, 54 p.

de Swiet, T. M., and P. N. Sen, 1994, Decay of nuclear magnetization by bounded diffusion in a constant field gradient: The Journal of Chemical Physics, v. 100, no. 8, p. 5597–5604.

Dodge, W. S. Sr., J. L. Shafer, and A. O. Guzman-Garcia, 1995, Core and log NMR measurements of an iron-rich, glauconitic sandstone reservoir: Society of Petrophysicists and Well Log Analysts (SPWLA) 36th Annual Logging Symposium, Paris, France, June 26-29, 1995, SPWLA-1995-O, 12 p.

Dunn, K.-J., D. J. Bergman, and G. A. LaTorraca, 2002, Nuclear magnetic resonance: Petrophysical and logging applications: Amsterdam, Elsevier, 316 p.

Foley, I., S. Farooqui, and R. Kleinberg, 1996, Effect of paramagnetic ions on NMR relaxation of fluids at solid surfaces: Journal of Magnetic Resonance. Series A., v. 123, no. 1, p. 95–104, doi:10.1006/jmra.1996.0218.

Gillis, P., and S. H. Koenig, 1987, Transverse relaxation of solvent protons induced by magnetized spheres: Application to ferritin, erythrocytes, and magnetite: Magnetic Resonance in Medicine, v. 5, no. 4, p. 323–345.

Gillis, P., F. Moiny, and R. A. Brooks, 2002, On T_2-shortening by strongly magnetized spheres: A partial refocusing model: Magnetic Resonance in Medicine, v. 47, no. 2, p. 257–263, doi:10.1002/mrm.10059.

Grunewald, E., and R. Knight, 2009, A laboratory study of NMR relaxation times and pore coupling in heterogeneous media: Geophysics, v. 74, no. 6, p. E215–E221, doi: 10.1190/1.3223712.

Hu ̈rlimann,M.D.,1998, Effective gradients in porous media due to susceptibility differences: Journal of Magnetic Resonance, v. 131, no. 2, p. 232–240, doi:10.1006 /jmre.1998.1364.

Hu ̈rlimann, M. D., A. Matteson, J. Massey, D. Allen, E. Fordham, F. Antonsen, and H.

Ruesla¨tten, 2004, Application of NMR diffusion editing as chlorite indicator: Petrophysics, v. 45, p. 414–421.
Jensen, J., and R. Chandra, 2000, NMR relaxation in tissues with weak magnetic inhomogeneities: Magnetic Resonance in Medicine, v. 44, no. 1, p. 144–156, doi:10.1002/1522- 2594(200007)44:1<144::AID-MRM21>3.0.CO;2-O.
Keating, K., 2014, A laboratory study to determine the effect of surface area and bead diameter on NMR relaxation rates of glass bead packs: Near Surface Geophysics, v. 12, no. 2016, p. 243–254, doi:10.3997/1873-0604.2013064.
Keating, K., and R. Knight, 2007, A laboratory study to determine the effect of iron oxides on proton NMR measurements: Geophysics, v. 72, no. 1, p. E27–E32, doi: 10.1190/1.2399445.
Keating, K., and R. Knight, 2008, A laboratory study of the effect of magnetite on NMR relaxation rates: Journal of Applied Geophysics, v. 66, no. 3–4, p. 188–196, doi: 10.1016/j.jappgeo.2007.09.001.
Keating, K., and R. Knight, 2010, A laboratory study of the effect of Fe (II)-bearing minerals on nuclear magnetic resonance (NMR) relaxation measurements: Geophysics, v. 75, no. 3, p. F71–F82, doi:10.1190/1.3386573.
Kenyon, B., R. Kleinberg, C. Straley, G. Gubelin, and C. Morriss, 1995, Nuclear magnetic resonance imaging— Technology for the 21st century: Oilfield Review, v. 7, p. 19–33.
Kenyon, W., 1997, Petrophysical principles of applications of NMR logging: Log Analyst, v. 38, p. 21–43.
Kenyon, W., P. Day, C. Straley, and J. Willemsen, 1988, A three-part study of NMR longitudinal relaxation properties of water-saturated sandstones: SPE Formation Evaluation, v. 3, no. 03, p. 622–636, doi:10.2118/15643-PA.
Kleinberg, R. L., S. A. Farooqui, and M. A. Horsfield, 1993a, T_1/T_2 ratio and frequency dependence of NMR re- laxation in porous sedimentary rocks: Journal of Colloid and Interface Science, v. 158, no. 1, p. 195–198, doi: 10.1006/jcis.1993.1247.
Kleinberg, R. L., and M. A. Horsfield, 1990, Transverse re- laxation processes in porous sedimentary rock: Journal of Magnetic Resonance, v. 88, p. 9–19.
Kleinberg, R. L., W. E. Kenyon, and P. P. Mitra, 1994, Mechanism of NMR relaxation of fluids in rock: Journal of Magnetic Resonance. Series A., v. 108, no. 2, p. 206–214, doi:10.1006/jmra.1994.1112.
Kleinberg,R.L., C.Straley, W.E.Kenyon, R.Akkurt, and S. A. Farooqui, 1993b, Nuclear magnetic resonance of rocks: T1 vs. T2: Society of Petroleum Engineers (SPE) Annual Technical Conference and Exhibition, Houston, Texas, October 3–6, 1993, SPE-26470-MS, 11 p., doi: 10.2118/26470-MS.
Kleinberg, R. L., and H. Vinegar, 1996, NMR properties of reservoir fluids: Log Analyst, v. 37, p. 20–32.
LaTorraca, G. A., K. J. Dunn, and D. J. Bergman, 1995, Magnetic susceptibility contrast effects on NMR T2 logging: Society of Petrophysicists and Well Log Analysts (SPWLA) 36th Annual Logging Symposium, Paris, France, June 26–29, 1995, SPWLA-1995-JJ, 8 p.
Levitt, M. H., 2008, Spin dynamics: Basics of nuclear magnetic resonance: Chichester, United Kingdom, John Wiley & Sons, 714 p.
Loucks, R. G., R. M. Reed, S. C. Ruppel, and D. M. Jarvie, 2009, Morphology, genesis,

and distribution of nanometer-scale pores in siliceous mudstones of the Mississippian Barnett Shale: Journal of Sedimentary Re- search, v. 79, no. 12, p. 848–861, doi:10.2110/jsr.2009.092.
Lowell, S., and J. E. Shields, 2013, Powder surface area and porosity, 3rd ed.: New York, Springer Science & Business Media, 234 p.
Matteson, A., J. P. Tomanic, M. M. Herron, D. F. Allen, and W. E. Kenyon, 1998, NMR relaxation of clay-brine mixtures: Society of Petroleum Engineers (SPE) Annual Technical Conference and Exhibition, New Orleans, Louisiana, September 27–30,1998, SPE-49008-MS, 7 p., doi:10.2118/49008-MS.
Meiboom, S., and D. Gill, 1958, Modified spin-echo method for measuring nuclear relaxation times: Review of Scientific Instruments, v. 29, no. 8, p. 688–691, doi: 10.1063/1.1716296.
Ruesla ̈tten, H., T. Eidsemo, C. Slot-Petersen, and J. White, 1998, NMR studies of an iron-rich sandstone oil reservoir: Proceedings of the 1998 International Symposium of the Society of Core Analysts, The Hague, The Netherlands, September 14–16, 1998, SCA 9821, 10 p.
Saidian, M., K. Livo, and M. Prasad, 2015, Effect of paramagnetic mineral content and distribution on surface relaxivity in organic-rich Niobrara and Haynesville shales (abs.), in R. V. Schneider, ed., SEG Technical Program Expanded Abstracts 2015: Tulsa, Oklahoma, Society Of Exploration Geophysicists, p. 2671–2676.
Senturia, S. D., and J. Robinson, 1970, Nuclear spin-lattice relaxation of liquids confined in porous solids: Society of Petroleum Engineers Journal, v. 10, no. 3, p. 237–244, doi:10.2118/2870-PA.
Sezginer, A., C. C. Mirth, G. Van Dort, M. Herron, N. Heaton, and R. Freedman, 1999, An NMR high- resolution permeability indicator: Society of Petrophysicists and Well Log Analysts (SPWLA) 40th Annual Logging Symposium, Oslo, Norway, May 30–June 3, 1999, SPWLA-1999-NNN, 12 p.
Song,Y.-Q., L.Venkataramanan, M.Hu ̈rlimann,M.Flaum, P. Frulla, and C. Straley, 2002, T1–T2 correlation spectra obtained using a fast two-dimensional Laplace inversion: Journal of Magnetic Resonance, v. 154, no. 2, p. 261–268, doi:10.1006/jmre.2001.2474.
Timur, A., 1968a, An investigation of permeability, porosity, and residual water saturation relationships: Society of Petrophysicists and Well Log Analysts (SPWLA) 9th Annual Logging Symposium, New Orleans, Louisiana, June 23–26, 1968, SPWLA-1968-vIXn4a2, 10 p.
Timur, A., 1968b, Effective porosity and permeability of sandstones investigated through nuclear magnetic resonance principles: Society of Petrophysicists and Well Log Analysts (SPWLA) 9th Annual Logging Symposium, New Orleans, Louisiana, June 23–26, 1968, SPWLA- 1968-K, 18 p.
Timur, A., 1969, Pulsed nuclear magnetic resonance studies of porosity, movable fluid, and permeability of sandstones: Journal of Petroleum Technology, v. 21, no. 06, p. 775–786, doi:10.2118/2045-PA.
Washburn, K. E., 2014, Relaxation mechanisms and shales: Concepts in Magnetic Resonance Part A, v. 43A, no. 3, p. 57–78, doi:10.1002/cmr.a.21302.
Washburn, K. E., and J. E. Birdwell, 2013, Updated methodology for nuclear magnetic resonance characterization of shales: Journal of Magnetic Resonance, v. 233, p. 17–

28, doi:10.1016/j.jmr.2013.04.014.
Washburn, K. E., J. E. Birdwell, J. D. Seymour, C. Kirkland, and S. J. Vogt, 2013, Low-field nuclear magnetic resonance characterization of organic content in shales: Proceedings of the 2013 International Symposium of the Society of Core Analysts, Napa Valley, CA, September 16–19, 2013, SCA2013-002, 12 p.
Whittall, K. P., M. J. Bronskill, and R. M. Henkelman, 1991, Investigation of analysis techniques for complicated NMR relaxation data: Journal of Magnetic Resonance, v. 95, p. 221–234.
Zhang, G. Q., G. J. Hirasaki, and W. V. House, 1998, Diffusion in internal field gradients: Proceedings of the 1998 International Symposium of the Society of Core Analysts, The Hague, The Netherlands, September 14–16, 1998, SCA-9823, 10 p.
Zhang, G. Q., G. J. Hirasaki, and W. V. House, 2001, Effect of internal field gradients on NMR measurements: Petro- physics, v. 42, p. 37–47.
Zhang, G. Q., G. J. Hirasaki, and W. V. House, 2003, Internal field gradients in porous media: Petrophysics, v. 44, p. 422–434.
Zhang, Q., S.-W. Lo, C. Huang, G. Hirasaki, R. Kobayashi, and W. House, 1998, Some exceptions to default NMR rock and fluid properties: Society of Petrophysicists and Well Log Analysts (SPWLA) 39th Annual Logging Symposium, Keystone, Colorado, May 26–28, 1998, SPWLA-1998-FF, 14 p.

CHAPTER 3

T_2 RELAXATION OF CLAY/BRINE MIXTURES

Obasi and Pashin 2018

To be submitted to Petroleum Geoscience

Boone Pickens School of Geology, Oklahoma State University, 105 Noble Research Center, Stillwater, OK 74078-3031.

ABSTRACT

Interpretation of nuclear magnetic resonance (NMR) logs, which are used to assess fluid saturation and mobility, from microporous shale reservoirs is a challenge for unconventional oil and gas exploration because it was developed for the characterization of macroporous sandstone and carbonate reservoirs and is not always accurate in shale. The partitioning of transverse relaxation time (T_2) distribution into irreducible and mobile fluids using a T_2-cutoff value is standard practice. However, in shale this approach does not always yield accurate results due to high clay contents, differential compaction, and magnetic minerals that can strongly influence the NMR log response. To effectively

characterize the NMR response of shale, the effects of clay common in shale need to be considered.

To begin addressing this issue, NMR experiments were designed to explore the effect of a range of clay minerals (illite, glauconite, chamosite, montmorillonite), on the NMR T_2 relaxation. These experiments were performed using pure minerals, saturated with brine. Slurries of brine and sediment were compacted in a centrifuge at pressures of 40 (2.75×10^5 Pa), 150 (1.03×10^6 Pa) and 600 pounds per square inch (psi), (4.14×10^6 Pa). A standard CPMG pulse sequence was performed on all samples at ten echo spacings ranging from 0.15 to 1.50 milliseconds. Results of NMR analysis indicate that transverse relaxation time (T_2) progressively shifted to shorter times as compaction increased, whereas surface area-volume-ratio increased for all mineral slurries investigated except montmorillonite, which exhibited significant reduction in water volume.

3.1 INTRODUCTION

Before now, NMR logging for evaluation of petrophysical properties such as porosity, pore size distribution, pore geometry, permeability, water saturation, clay-bound water fraction, and wettability conditions, has been used for of macroporous sandstone and carbonate formations which are generally described as conventional resource reservoirs (Bryar et al., 2000). Although ‘unconventional’ resource reservoirs have no generalized definition, they are typically reserved for reservoirs that lack one or more requirements of conventional reservoirs, which do not produce economic rates of

hydrocarbons without stimulation and they include: oil-shale formations, shale gas, gas hydrates, tight-gas sandstones and heavy-oil sandstones (Passey et al., 2010; Washburn and Birdwell, 2013). Recently, there has been increased development of unconventional petroleum resources, which reside in shale, due to the emerging energy demand globally. Therefore, a practical understanding of the role of clays in rapid NMR signal relaxation will help to effectively interpret NMR logs in shale.

NMR T_2 distribution estimates clay bound water, which is used in determining water saturation from resistivity, based on a cutoff, at less than 3 milliseconds (Straley et al., 1987). The study by Matteson et al. (2000) of clay/brine mixtures of kaolinite, illite, smectite and glauconite, did not yield any significant different between the clay types studied, with shifting peak positions depending on compaction. However, Fleury et al. (2013), observed small relaxation time in clays, with these being close to the value for quartz surfaces, and not as a result of high surface relaxivity (explained later) induced by paramagnetic impurities, but rather are due to high specific surface area. Additionally, Slijkerman and Hofman (1998) demonstrated that diffusion of water protons in a porous material, is not dependent on surface relaxivity, but is restricted by the size of the pore.

For a water-saturated porous medium, the NMR relaxation experiment consists of observing hydrogen nuclei (protons) in pore water align with the static magnetic field, then are perturbed by the application of a radio frequency (RF), emitting a measurable signals as they relax back to equilibrium, after the RF is removed (Keating, 2014). The surface-area-to-volume ratio of water wet pore system is related to the measured T_2 relaxation rate, and has a proportionality constant called surface relaxivity. This aforementioned relationship provides the link to use NMR data to estimate permeability

(e.g., Vogeley and Moses, 1992; Legchenko et al., 2002; Keating and Knight, 2006) and (e.g., Timur, 1969; Yaramanci et al., 2002; Keating and Knight 2006) pore size distribution. In a single pore, the mean NMR T_2 relaxation time of water is the sum of three relaxation times (Brownstein and Tarr, 1979; Keating and Knight, 2006):

$$T_{2ML} = T_{2B} + T_{2S} + T_{2D} \quad (23)$$

Where T_2 relaxation time is the transverse relaxation time, usually higher than bulk relaxation (T_{2B}), being enhanced by surface (T_{2S}) and diffusion (T_{2S}) relaxation time mechanisms. The interaction that occurs between water and paramagnetic sites on pore solid surface (i.e., atoms with unpaired electrons) (e.g. surface relaxivity, ρ_2), and magnetic minerals with high values of magnetic susceptibility are the two factors that can affect the relationship between NMR relaxation rate and S/V. (Keating and Knight, 2010). The NMR T_2 relaxation time expressed above is valid for samples in fast diffusion regimes where the travel to and relaxation at solid surface by protons within the time interval NMR experiment is assumed (Senturia and Robinson, 1970; Brownstein and Tarr, 1979, Keating and Keating, 2006).

The objective of this study is to determine the effects of compaction on T_2 relaxation of clays and apply the result toward enhancing reservoir petrophysical comprehension. In order to accomplish this goal, we designed a set of experiments that examined the NMR T_2 relaxation of clay/brine mixtures at various compaction states. The monomineralic samples used ensured that NMR T_2 relaxation behavior was evaluated, and through compaction, volume-to-surface ratio was easily varied. We chose to study four clays commonly found in oil-bearing sedimentary environments: chamosite, illite, glauconite and montmorillonite.

3.2 MATERIALS AND METHODS

3.2.1 Sample Preparation and Characterization

All four samples used in this study were acquired from three mineral repositories. The samples include illite, glauconite, chamosite and montmorillonite. Illite (from Wards Scientific) and montmorillonite (from Source Clays Repository) were received as powder (particle size < 38 μm or 1.25 x 10^{-4} ft.), whereas glauconite (from Wards Scientific) and chamosite (from Excalibur Mineral Corporation) received as bulky samples were crushed and/or sieved with a 300μm ($1.0x10^{-3}$) size mesh. Bruker D8 Advance X-Ray Diffractometer was used to verify mineralogy and their elemental composition was obtained using Thermo Scientific X-Ray Fluorescence instrument. The volumetric magnetic susceptibility (MS) for all the samples was measured at a low frequency of 0.465 kHz (Bartington MS2 Magnetic Susceptibility System). The specific surface area S_s, which is defined as the surface area normalized by the sample mass, was estimated with the Brunauer-Emmett-Teller pore filling model using N_2 as an adsorbate (e.g., Lowell and Shield, 2013). A 125-g/L NaCl brine was used to saturate all samples and the mineral/brine slurry was centrifuged to compact the solid phase but the liquid phased was decanted. A 1:2 ratio by mass was used to prepare all mineral-brine slurries. The slurries were compacted using Eppendorf Centrifuge 5804 at 40 (2.75 x 10^5 Pa), 150 (1.03 x 10^6 Pa) and 600 pounds per square inch (4.14 x 10^6 Pa) respectively, order to simulate variable subsurface pressures conditions in a similar method as performed in (Matteson et al., 1998). Residual air bubbles were expelled during compaction intervals with a Vortex-2 Gene vibrating instrument.

3.2.2 Nuclear Magnetic Resonance Measurement

2 MHz Magritek Rock Core Analyzer was used to collect NMR relaxation data running a CPMG (Carr- Purcell-Meiboom-Gill) pulse sequence. Data for each sample was collected at 10 echo times: 150, 200, 300, 400, 500, 600, 800, 1000, 1200, and 1500 micro-seconds (μs) for each of the compacted states of the samples, with delay stacks being minimum three times the relaxation time. Number of echoes collected was 40 for montmorillonite, 50 for chamosite and illite whereas 60 was collected for glauconite. Each raw signal for a T_2 relaxation time distribution was inverted using a regularized least square algorithm based on Whittall et al. (1991). Measurements were repeated multiple times for consistency of data. S*por* was computed from an equation according to Keating and Knight (2010). Signal to noise ratio was enhanced by stacking the data 256 times. A constant temperature of 30^0C was maintained for all measurements during the entire measurement in order to eliminate temperature variations and avoid changes in the NMR response.

3.3 RESULTS & DISCUSSION

This study examined the contributions of incremental compaction of mineral samples common in shale on relaxation. The concentration of Fe and Mn in each of the samples, obtained with XRF elemental analysis, are listed along with the oxides is presented in Table 3-1. The total iron concentration measured from 7% in illite to 23.5% in glauconite. The concentration of manganese measured 0.05%, 0.5% and 0.1% in illite, chamosite and glauconite but was undetected in montmorillonite. The weight percentages

of Fe and Mn were determined, as a basic quality assurance measure, to be consistent with what literature reported (Carmichael, 1982; Dearing, 1994; Dodge et al., 1995; Matteson et al., 1998, G.Q. Zhang et al., 1998; Keating and Knight, 2010). The XRD results confirmed the mineralogy of the entire sample. Volumetric magnetic susceptibility values also are listed in Table 3-1. The values range from -9 X 10^{-6} (Hurlimann, 1998) to 438 X 10^{-6} [SI] standard international (SI) units. High weight percent iron in minerals did not necessarily render high magnetic susceptibility values in minerals studied (Figure 3-1). Chamosite did not have the highest iron concentration; it has the highest manganese concentration (0.5 wt. %), and highest magnetic susceptibility 438 X 10^{-6} [SI]. The values of specific surface area for each sample ranges from 0.2 m^2/g for chamosite to 92 m^2/g for montmorillonite, and are reported in Table 3-1.

Table 3-1: Chemical and physical properties of minerals.

Mineral Properties	Surface Area (m^2/g)	Magnetic Susceptibility (x 10^{-6} SI)	Fe (wt.%)	Mn (wt.%)	S (wt.%)	SiO_2 (wt.%)	Al_2O_3 (wt.%)	MgO (wt.%)	K_2O (wt.%)
Illite Maplewood Shale, Rochester NY	19.0	217.0	7.0	0.05	0.3	48.0	27.0	2.4	5.0
Chamosite Fremont Co., Wyoming	2.0	438.0	21.0	0.48	0.2	28.0	21.0	4.3	0.5
Glauconite Birmingham, New Jersey	53.0	57.0	23.5	0.1	2.1	31.0	9.3	<LOD	3.4
Montmorillonite Gonzales Co., Texas	92.0	8.0	1.5	<LOD	0.05	60.5	18.0	1.7	0.1

Abbreviations: MS = magnetic susceptibility; SI = standard international units. LOD = Limit of Detection

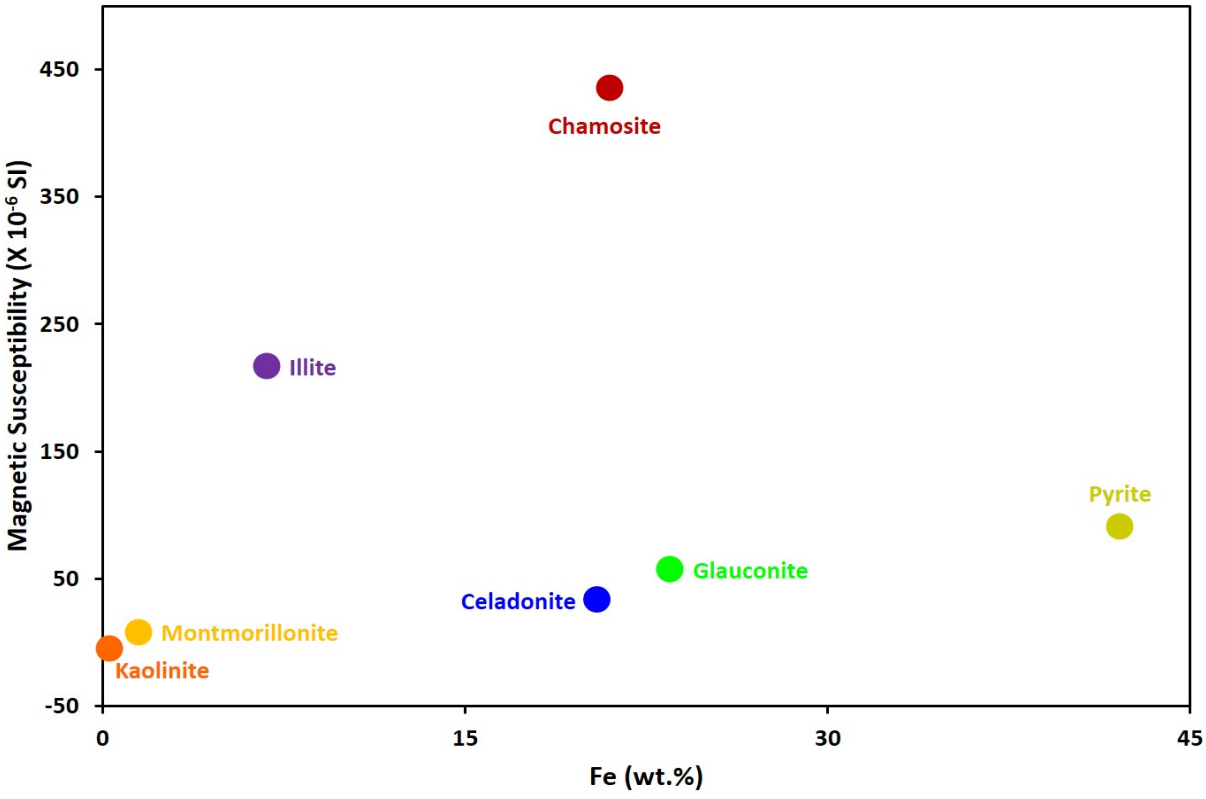

Figure 3-1: Relationship between magnetic susceptibility and weight percent iron in mineral samples.

The T_2 relaxation distributions of incrementally compacted samples are presented in Figure 3-2. Evidence of continued reduction in T_{2ML} relaxation time was observed as compaction of the slurries increased. The number of protons in the measured sample, which is proportional to the initial signal amplitude and can be used to estimate water volume, and porosity in a saturated sample (Keating, 2014). The T_{2ML} distributions shown in Figure 3-2 indicate a reduction in water volume or porosity as sample compaction increased. Compacting the samples from 150 (1.03×10^6 Pa) to 600 psi (4.14×10^6 Pa), the magnitude of water volume reduction was less significant in chamosite and but drastic for montmorillonite (Figure 3-2). T_{2ML} relaxation time versus incremental compaction and the computed surface area-volume ratio S_{por}, is shown in the plot on Figure 3-3. The T_{2ML} relaxation time decreases with increasing compaction for all samples except montmorillonite (Figure 3-3). The plot of surface area-volume ratio versus compaction indicates that surface area-volume ratio increases with increasing compaction, hence accounting for the decrease of T_2 relaxation time (Figure 3-3).

Incrementally compacting the samples at different pressures establishes a negative correlation between the log-mean T_{2ML} relaxation time versus pressure whereas the correlation between surface area-volume-ratio versus pressure was positive. Transverse relaxation time (T_2) progressively shifted to shorter times as pressure increased, whereas surface area-volume-ratio increased for all minerals except montmorillonite (Figure 3-3). These observations demonstrate that pore volume-to-surface ratio is proportional to the relaxation time. Matteson et al. (1998), stated that iron content correlates with the surface relaxivity of clays, however, there was no evidence from clays studied, to validate that statement. In our study, the T_2 peak positions are, from shortest to longest relaxation time,

chamosite, illite and glauconite (not variation between the two), then montmorillonite, with weight percent iron from 21, 7, 23.5 and 8 respectively.

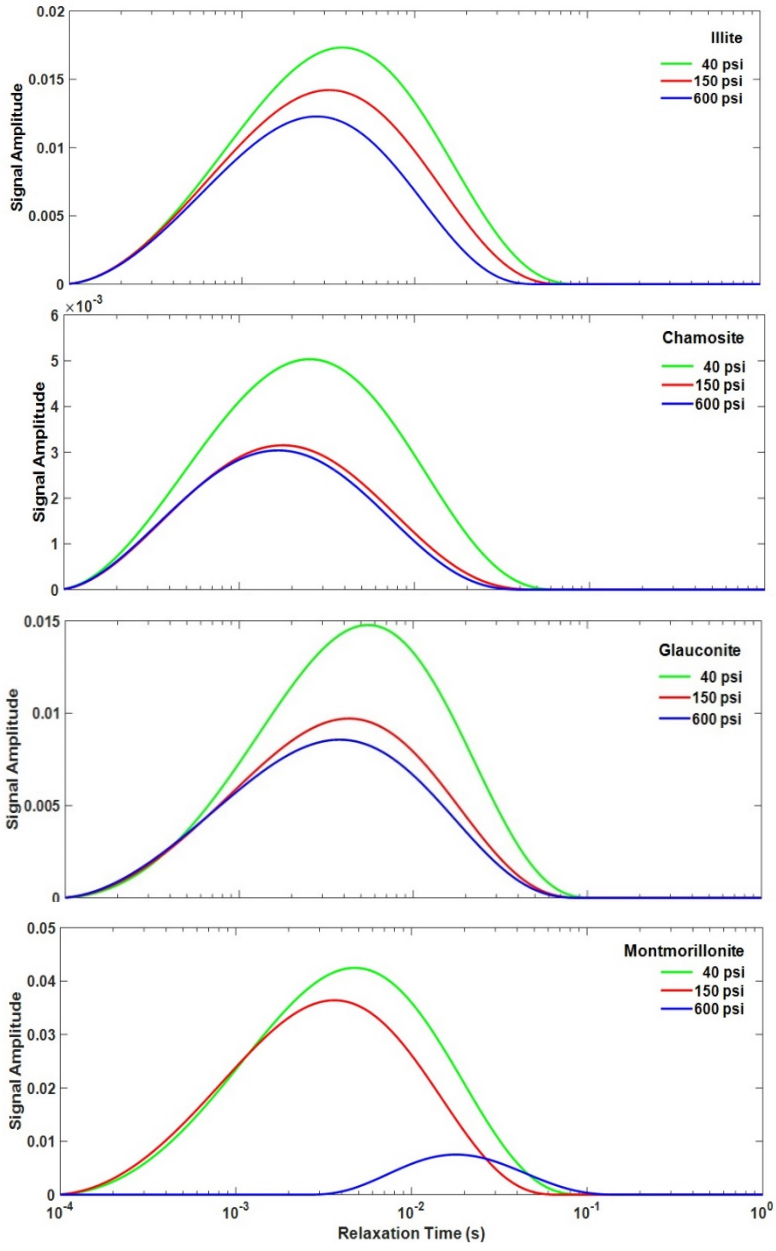

Figure 3-2: Transverse T_2 relaxation distribution plots showing relaxation times at different levels of compaction.

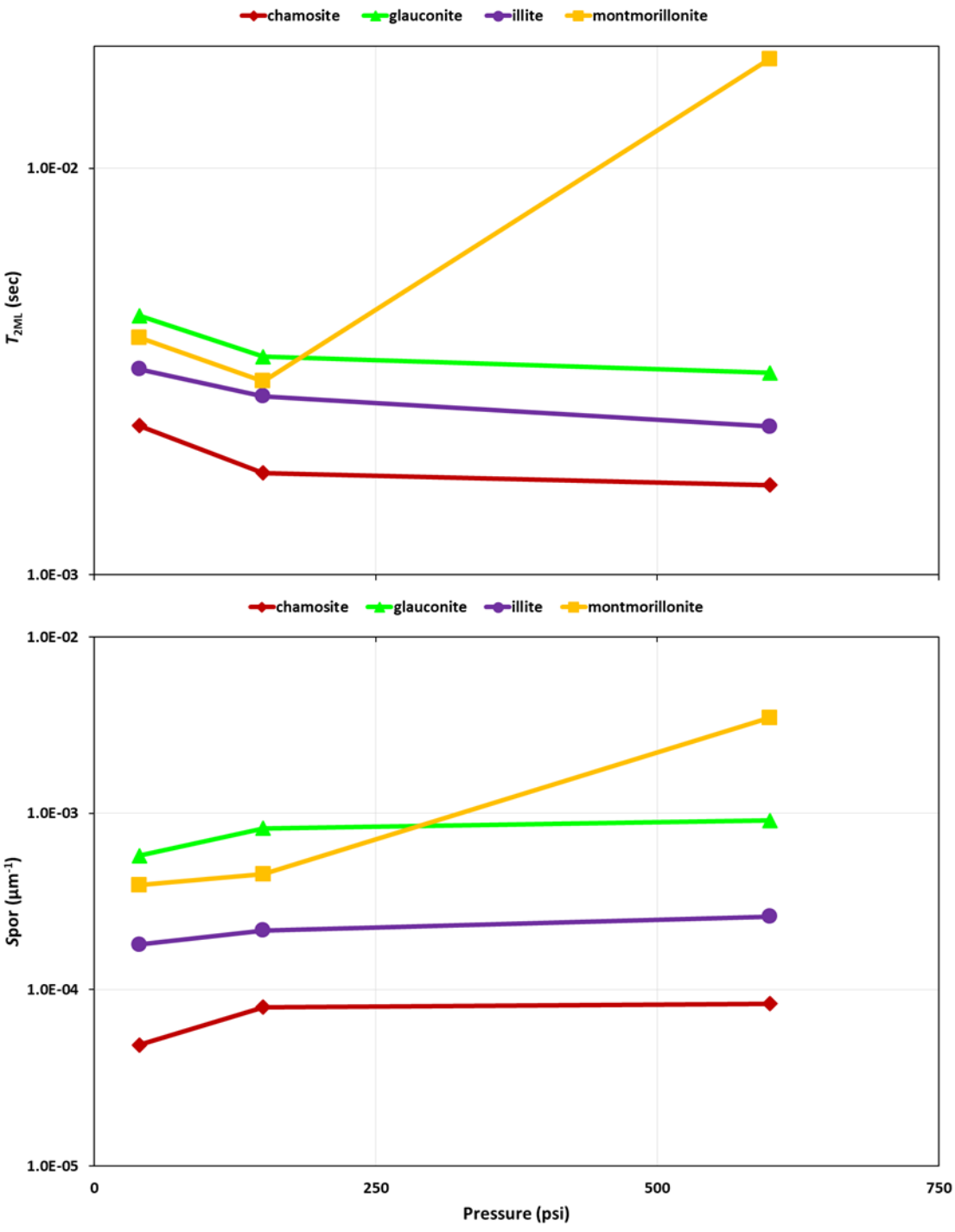

Figure 3-3: (a) A graph of T_{2ML} versus incremental compaction pressure. **(b)** A graph of computed *Spor* versus incremental compaction pressure.

3.4 CONCLUSION

This paper presented NMR measurement of brine mixture of four common clay minerals, including montmorillonite, glauconite, illite and chamosite as a function of compaction. The NMR signal progressively decayed at a faster relaxation rate, to shorter times as compaction, and pore volume-to-surface-ratio, increased. Although earlier work suggested that the T_2 relaxation rate of the hydrogen proton in the mixture might correlate with the iron content, no distinct evidence was found from this study to strongly validate their assertion.

REFERENCES CITED

Brownstein, K. R., and C. Tarr, 1979, Importance of classical diffusion in NMR studies of water in biological cells: Physical review A, v. 19, p. 2446.

Bryar, T. R., C. J. Daughney, and R. J. Knight, 2000, Paramagnetic effects of iron (III) species on nuclear magnetic relaxation of fluid protons in porous media: Journal of magnetic resonance, v. 142, p. 74-85.

Carmichael, R. S., ed.,, CRC handbook of physical properties of rocks: Boca Raton, Florida, CRC Press, v.2, 360 p.

Dearing, J., 1994, Environmental magnetic susceptibility: Using the Bartington MS2 system. Kenilworth, Chi Publ.

Dodge, W., J. L. Shafer, and A. O. Guzman-Garcia, 1995, Core and log NMR measurements of an iron-rich, glauconitic sandstone reservoir: SPWLA 36th Annual Logging Symposium.

Fleury, M., E. Kohler, F. Norrant, S. Gautier, J. M'Hamdi, and L. Barré, 2013, Characterization and quantification of water in smectites with low-field NMR: The Journal of Physical Chemistry C, v. 117, p. 4551-4560.

Hürlimann, M. D., 1998, Effective gradients in porous media due to susceptibility differences: Journal of Magnetic Resonance, v. 131, p. 232-240.

Keating, K., 2014, A laboratory study to determine the effect of surface area and bead diameter on NMR relaxation rates of glass bead packs: Near Surface Geophysics, v. 12, p. 243-254.

Keating, K., and R. Knight, 2006, A laboratory study to determine the effect of iron oxides on proton NMR measurements: Geophysics, v. 72, p. E27-E32.

Keating, K., and R. Knight, 2010, A laboratory study of the effect of Fe (II)-bearing minerals on nuclear magnetic resonance (NMR) relaxation measurements: Geophysics, v. 75, p. F71-F82.

Legchenko, A., J.-M. Baltassat, A. Beauce, and J. Bernard, 2002, Nuclear magnetic resonance as a geophysical tool for hydrogeologists: Journal of Applied Geophysics, v. 50, p. 21-46.

Legchenko, A., J. M. Baltassat, A. Bobachev, C. Martin, H. Robain, and J. M. Vouillamoz, 2004, Magnetic resonance sounding applied to aquifer characterization: Groundwater, v. 42, p. 363-373.

Lowell, S., and J. E. Shields, 2013, Powder surface area and porosity, v. 2, Springer Science & Business Media.

Matteson, A., J. Tomanic, M. Herron, D. Allen, and W. Kenyon, 1998, NMR relaxation of clay-brine mixtures: SPE Annual Technical Conference and Exhibition.

Passey, Q. R., K. Bohacs, W. L. Esch, R. Klimentidis, and S. Sinha, 2010, From oil-prone source rock to gas-producing shale reservoir-geologic and petrophysical characterization of unconventional shale gas reservoirs: International oil and gas conference and exhibition in China.

Senturia, S. D., and J. Robinson, 1970, Nuclear spin-lattice relaxation of liquids confined in porous solids: Society of Petroleum Engineers Journal, v. 10, p. 237-244.

Slijkerman, W., and J. Hofman, 1998, Determination of surface relaxivity from NMR diffusion measurements: Magnetic resonance imaging, v. 16, p. 541-544.

Straley, C., A. Matteson, S. Feng, L. M. Schwartz, W. E. Kenyon, and J. R. Banavar, 1987, Magnetic resonance, digital image analysis, and permeability of porous media: Applied Physics Letters, v. 51, p. 1146-1148.

Timur, A., 1969, Pulsed nuclear magnetic resonance studies of porosity, movable fluid, and permeability of sandstones: Journal of Petroleum Technology, v. 21, p. 775-786.

Vogeley, J. R., 1992, 1HNMR relaxation and rock permeability: Geochimica et Cosmochimica Acta, v. 56, p. 2947-2953.

Washburn, K. E., and J. E. Birdwell, 2013, Updated methodology for nuclear magnetic resonance characterization of shales: Journal of Magnetic Resonance, v. 233, p. 17-28.

Whittall, K. P., M. J. Bronskill, and R. M. Henkelman, 1991, Investigation of analysis techniques for complicated NMR relaxation data: Journal of Magnetic Resonance (1969), v. 95, p. 221-234.

Yaramanci, U., G. Lange, and M. Hertrich, 2002, Aquifer characterisation using Surface NMR jointly with other geophysical techniques at the Nauen/Berlin test site: Journal of Applied Geophysics, v. 50, p. 47-65.

Zhang, G. Q., G. J. Hirasaki, and W. V. House, 1998, Diffusion in internal field gradients: International Symposium of the Society of Core Analysts, Paper.

CHAPTER 4

NMR AND OTHER PETROPHYSICAL BEHAVIORS OF ORGANIC-RICH WOODFORD SHALE, NORTHERN SHELF, ANADARKO BASIN

Obasi, Pashin, Puckette, and Foltz 2018

To be submitted to Marine and Petroleum Geology

Boone Pickens School of Geology, Oklahoma State University, 105 Noble Research Center, Stillwater, OK 74078-3031.

ABSTRACT:

The Devonian shale Woodford Shale is source to vast global oil and gas reserves. Signature petrophysical response of the Woodford comprises high resistivity, low bulk density, elevated gamma response, and low photoelectric absorption factor. NMR measurement is a non-invasive tool for obtaining lithology-independent porosity and characterizing other reservoir properties in conventional sandstone or carbonate reservoirs, but is problematic in unconventional shale reservoirs due to its small pore size, low permeability, and the presence more paramagnetic impurities than with the conventional reservoirs.

In this study, we measured NMR relaxation and obtained magnetic susceptibility, specific surface area and elemental composition measurements in the Woodford. Furthermore, we compared NMR based approach of evaluating the Woodford to that obtained with traditional petrophysical data including bulk and grain density, neutron porosity, resistivity, photoelectric absorption factor and gamma-ray activity provided by Weatherford Laboratories. We conclude that integrating NMR data into traditional petrophysical data, will provide better insight into unconventional resource evaluation.

4.1 INTRODUCTION

The Woodford Shale is a significant petroleum reservoir and is recognized as the primary source rock in the southern Midcontinent of North America (Kirkland et al., 1992). The Woodford Shale and coeval Devonian shale formations, such as the Marcellus (Pennsylvania, West Virginia), Ohio (Ohio, Kentucky), Chattanooga (Tennessee, Kentucky), and Bakken (North Dakota), are thought to have sourced nearly 8% of the world's oil and gas reserves (Ulmishek and Klemme, 1990). The Woodford Shale in Oklahoma and Kansas is well studied for its source rock potential (Kirkland et al., 1992) and has been drilled for oil and gas production for more than a decade (Cardott, 2012). Typical petrophysical response of the Woodford comprises low bulk density, low photoelectric absorption factor, high resistivity, and elevated gamma response (Lewis et al., 2004). While the Woodford Shale is the focus of exploration, the petrophysical characteristics of the formation are incompletely known.

Nuclear magnetic resonance (NMR) is a valuable tool for determining pore-size distribution based on the distribution of relaxation times (Kenyon et al., 1995; Latour et al., 1995; Hürlimann et al., 2004), from which reservoir properties such as porosity, permeability, bound water content, free fluid content and total saturation can be derived (Kleinberg, 1994; Allen et al., 2000). The advantages of NMR over other wireline surveys are that it can yield a continuous log of permeability, can provide lithology-independent porosity, is non-invasive and does not require radioactive source (Kenyon et al., 1995; Daughney et al., 2000; Westphal et al., 2005; Washburn, 2014). Although NMR measurement is a superior tool for characterizing reservoir properties in conventional reservoirs like sandstone or carbonate, it is more problematic in unconventional shale reservoirs because of small pore size, low permeability (nanodarcy-microdarcy), and the presence paramagnetic mineral components (Loucks et. al., 2009; Washburn, 2014). Shale often contains framboidal pyrite that is capable of hosting approximately 20-30% intracrystalline porosity (Kleinberg et al., 1994; Washburn, 2014). Much of the iron in shale is associated with framboidal pyrite, whereas very little is contained in the organic matter (Acholla and Orr, 1993; Mercer et al., 1993). Whether present in aqueous states or mineralogical forms, iron will affect NMR relaxation rates (Keating and Knight, 2010), hence the motivation to better comprehend NMR behavior of organic-rich Woodford Shale.

NMR relaxation measurement, as employed in petrophysical studies, entails placing a fluid-saturated porous medium in the presence of static magnetic field. The magnetic moments of hydrogen nuclei (proton) in the fluid steadily precess around the applied magnetic field. A radiofrequency pulse is then applied to perturb magnetic spin

away from the applied magnetic field. Once the radiofrequency pulse is removed, the NMR signal returns to equilibrium (i.e., relaxes) via two simultaneous relaxation mechanisms. The first refers to the time taken for the perturbed magnetization to relax to thermal equilibrium, known as the longitudinal T_1 relaxation. The second is the time it takes for spins to return from the ordered state induced by an external magnetic field to the natural, disordered state known as transverse T_2 relaxation time (Levitt, 2001; Keating and Knight, 2010; Washburn et al., 2013). NMR surface relaxivity, which relates NMR $T_{1,2}$ to pore size, can also be evaluated through digital image analysis (Straley et al., 1987), or acquired from digitized thin sections (Howard et al., 1993). Whereas pore size distribution obtained by estimating average pore radius from the surface area measured by the Brunauer-Emmett-Teller adsorption method (Keating and Knight, 2010), can be used to substantiate NMR-based measurements, they are unavailable for downhole logging and are prone to the often ignored limitations of measurement scale that are encountered in general usage (e.g., Gallegos et al., 1987).

This research is designed to measure the NMR attributes across 36-ft of the Woodford Shale in a core from Barber County, Kansas. The focus of this research is to better understand the depositional and diagenetic properties of the Woodford Shale using NMR petrophysical data obtained in the Woodford Shale core from Barber County Kansas. By comparing selected conventional methods (e.g. neutron porosity, density, gamma ray, and resistivity measurements) of petrophysical analysis to the NMR approach, drawn inferences will be applied to improve on existing methods of petrophysical evaluation of the Woodford hydrocarbon resource.

4.2 THEORY AND BACKGROUND

4.2.1 Woodford Shale

The Woodford Shale has a distinct signature in geophysical well logs because of elevated gamma count. This is the result of high concentrations of uranium, which causes gamma count to exceed 150 API units (Paxton et al., 2006). In general, the environmental and depositional conditions that facilitate concentrating uranium in sediments, slow diffusion rates of uranium out of seawater under anoxic conditions, also favor the preservation of organic matter, confirming the conditions during deposition (Lüning and Kolonic, 2003).

The Woodford Shale contains abundant silica in the forms of amorphous silica cement, silt particles, and siliceous microfossils, including radiolaria (Kirkland et al., 1992; Roberts and Mitterer, 1992; Schieber et al., 2000). The Woodford is rich in pyrite and marcasite pyritized burrows which, based on Lobza and Schieber (1999), supports the premise that life was able to exist at least episodically within this normally anoxic environment. Horizontal pyrite laminae also occur, which could indicate shallow erosion surfaces, change in organic material, or an interruption of primary sedimentary fabric due to bioturbation (Droser and Bottjer, 1986; Schieber, 1998).

Magnetic susceptibility (χ) is a measure of how rocks such as shale develop magnetic moment when exposed to an external magnetic field. A rock having a positive χ value is paramagnetic, whereas one with a negative χ value is diamagnetic (Levitt, 2008). Iron-bearing minerals are typically paramagnetic, whereas those lacking iron are typically

diamagnetic (G. Q. Zhang et al., 1998). Wedepohl (1971) determined the chemical composition of most shale and clay, and observed that they contain 3% Fe_2O_3 and 4% FeO on average. By contrast, sandstone typically has low iron content on the order of 1% (Kleinberg and Vinegar, 1996). G. Q. Zhang et al (1998) demonstrated that iron-rich clay with high magnetic susceptibility can induce strong internal field gradients, which shorten T_2 relaxation time. Foley et al. (1996) and Bryar et al. (2000) demonstrated that, for any given mineral, iron concentration on the surface of a solid is proportional to its rate of relaxation.

4.2.2 Nuclear Magnetic Resonance Relaxation Theory

A summary of NMR theory is presented here; comprehensive reviews are available in several publications (Bloembergen et al., 1948; Kleinberg et al., 1994; Kenyon, 1997; Coates et al., 1999; Dunn et al., 2002). In this study, the arithmetic mean of log $T_{1,2}$ ($T_{1,2ML}$), used to represent the relaxation behavior of the rock samples, was calculated from the distribution of relaxation times, assuming a case of fast diffusion limit for each single pore (Senturia and Robinson, 1970; Brownstein and Tarr, 1979; Keating and Knight, 2006) and are given by

$$T_{1ML}^{-1} = T_{1B}^{-1} + \rho_1 \left(\frac{S}{V}\right) \tag{24}$$

$$T_{2ML}^{-1} = T_{2B}^{-1} + \rho_2 \left(\frac{S}{V}\right) + \frac{D}{12} (\gamma G t_E)^2 \tag{25}$$

Here, $T_{1,2B}^{-1}$ is the relaxation rate of the bulk water, $\rho_{1,2}$ is the surface relaxivity, γ is the gyromagnetic ratio of the hydrogen proton, D is the self diffusion coefficient, $\frac{S}{V}$ is the

surface-area-to-volume ratio (inversely proportional to the pore radius r_{pore}), and G is the average gradient strength. In general, T_1 measurements are challenging with borehole or surface instruments because they have longer measurement times than T_2, and are not readily repeated when logging across bedding interfaces (Kleinberg et al., 1993b; LaTorraca et al., 1995; Kleinberg and Vinegar, 1996; Bachman et al., 2007; Grunewald and Knight, 2009). Therefore, T_2 is typically the basis for NMR downhole field applications and are the focus of this article.

According to Grunewald and Knight (2009), in most geologic materials with low magnetic susceptibility, surface relaxation dominates, so that the expression for T_2^{-1} is reduced to,

$$T_2^{-1} = \rho_2 \left(\frac{S}{V}\right). \tag{26}$$

Whereas, in Keating and Knight (2008) (S/V) or (S_{por}) is described by

$$S_{por} = \frac{S}{V} = \frac{S_S m_S}{V_w} \tag{27}$$

where m_s is the mass of the sample, S_s is the specific surface area normalized by the sample mass and V_w is the volume of water in the sample, which also represents the pore space volume V (Keating and Knight, 2010).

4.2.3 Longitudinal Relaxation Time to Transverse Relaxation Time Correlation

The T_1/T_2 correlation plot is an important tool in the study of the molecular relaxation (Kleinberg and Horsfield, 1990; Song et al., 2002; Anand and Hirasaki, 2008). A T_1/T_2 plot greater than unity for a single, non-viscous fluid system, may suggest the presence of magnetic field inhomogeneities in a porous medium and the dependence of the relaxation

rate (T_2^{-1}) on the t_E^2 (Kleinberg et al., 1993a, b; Foley et al., 1996; Anand and Hirasaki, 2008). A plot of T_{2ML}^{-1} versus t_E^2 may generate a straight line with a slope equal to $\frac{D(\gamma G)^2}{12}$; and if positive slope, indicates the presence of internal gradient effect on diffusion relaxation (i.e. $G \neq 0$) (Anand and Hirasaki, 2008; Keating and Knight, 2008; Keating, 2014). In this study, it is suspected that high amounts of internal magnetic field gradients (i.e. its length scale larger than the molecular diffusion length), may affect T_2 relaxation rate and shorten T_{2ML} (G. Q. Zhang et al., 1998; Anand and Hirasaki, 2008).

4.3 MATERIALS AND METHODS

4.3.1 Sample Preparation and Characterization

A core of the Woodford Shale was acquired from Tug Hill Operating, Incorporated. The core has a length of 11 m (36 ft.) and it was retrieved from the Matthews 2-8H well in Barber County Kansas. Thirteen samples were obtained from the core at approximately 1.0- to 1.2- m (3- to 4- ft.) intervals in the Woodford Shale to conduct primary petrophysical measurements (Figure 3-1). In this study, the mineralogical composition of the Woodford was verified by XRD and was plotted on ternary modified after Loucks et al. (2012). The reservoir properties such as porosity and permeability, fluid saturation, grain density, bulk density, spectral gamma ray, and total organic carbon (TOC), were all determined in a laboratory. The brittleness index, which is a measure of the volumetric fraction of rigid grains as part of the entire volume of the rock matrix (Herwanger et al., 2015), was also determined. All the aforementioned

physical and petrophysical parameters were determined and provided by Weatherford Laboratories.

The Woodford core was described using standard stratigraphic and sedimentologic procedures; key variables such as rock type, color, and texture, as well as physical, biological, and diagenetic structures. The elemental composition of the samples were measured using a Niton ™ XL 3t GOLDD hand-held x-ray fluorescence (XRF) device and test stand, in order to ascertain the amount of Fe or other paramagnetic impurities in the samples. The volumetric magnetic susceptibility (MS), for all the samples was measured using a Bartington MS2 Magnetic Susceptibility System. These measurements were made at 0.465 kHz frequency. The specific surface area S_s, defined as the surface area normalized by the sample mass, was measured using the Brunauer-Emmett-Teller pore filling model with N_2 as an adsorbate (e.g., Lowell and Shield, 2013). The effective hydraulic radius R, of the reservoir's pore system was calculated, and it is defined as the ratio of the pore volume V_p to the grain fluid interfacial area S, and serves as a critical parameter for permeability estimation equations i.e., $R = V_p/S$ (Goode and Sen, 1988).

4.3.2 Nuclear Magnetic Resonance Measurement Procedure

To investigate the NMR response of the Woodford, NMR relaxation data were collected with 2-MHz Magritek Rock Core Analyzer using a Carr-Purcell-Meiboom-Gill (CPMG) pulse sequence. Data for each sample were collected at 10 echo times, specifically 150, 200, 300, 400, 500, 600 800, 1000, 1200, and 1500 μs; with the delay

time between stacks exceeding 3 times the relaxation time. For each sample, 50 echoes were collected. The T_{2ML} for short and long echo time (t_E = 150 and 1500 μs) relaxation distributions were calculated for each sample. The surface-area-to-volume ratio (S_{por}) was however, determined using the equation from Keating and Knight (2010). Average T_{2ML}^{-1} data and specific surface area were used to calculate the surface relaxivity of the lower Woodford zone. Each measured magnetization decay signal used to develop a T_2 relaxation time distribution was inverted using a regularized non-negative least squares algorithm after Whittall et al. (1991). Using this method, the data were fitted to a distribution of 160 logarithmically spaced T_2 values ranging from 10^{-4} to 10^{1} s. Next, the inverted model was regularized for smoothness and minimization of inversion artifacts. The mean log relaxation time, T_{2ML}, was used to represent the NMR relaxation behavior of the samples. This variable is expressed as the sum of the bulk, surface, and diffusion T_2 relaxation rates. The Longitudinal T_1 measurement for each sample was performed using an inversion recovery sequence.

In order to verify the presence of magnetic field inhomogeneities, T_1/T_2 ratio was measured according to Kleinberg and Horsfield (1990); Song and others (2002; Anand and Hirasaki (2008). The tau ratio τ_1/τ_2 varied logarithmically from a minimum of 0.2 to 1000 ms. τ_1 refers to the time period over which the spin magnetization decays along the ⧵ axis. During τ_2, the decay is due to T_2. A plot of the T_2 logarithmic mean relaxation (T_{2ML}^{-1}) versus square of echo spacing (t_E^2) was used to validate the presence of internal gradient (due to magnetic susceptibility contrasts) (i.e. $G \neq 0$) if positive slope (Anand and Hirasaki, 2008; Keating and Knight, 2008; Keating, 2014;). All the data were stacked 256 times, and a signal-to-noise ratio of 200 was achieved for all T_1, T_2, and T_1-T_2

measurements. Also, all measurements were made at 30°C to avoid changes in the NMR response due to variations in temperature. Replicate measurements were made for each sample in order to verify repeatability and control experimental error.

4.4 RESULTS

4.4.1 Core Description

Foltz (2015) subdivided the Woodford in this core into the lower section from 4876 to 4860 ft. as the lower pyrite-rich (LPR) zone or Lower Woodford and the upper pyrite-rich (UPR) zone or Upper Woodford from 4859-4838 ft. based on the Woodford Shale in the Matthews core visual description. The lower pyrite-rich (LPR) zone is assessed to be of superior reservoir quality and Weatherford Laboratories conducted additional petrophysical measurements from the zone (between 4874-4862 ft.). This LPR zone contains pyrite laminae, pyrite nodules, disseminated silt-sized pyrite, and a few pyrite bands at 4860–4867 ft. (Figure 4-1). Horizontal zones of concentrated silt-sized pyrite occur at 4874 and 4863 ft., but the pyrite is not abundant enough to be defined as a layer. A large pyrite nodule occurs at 4872 ft. that is 1 x 2 cm, but all other nodules are less than 1-cm. Pyrite laminae are usually less than 0.1 cm and the defining characteristic of this interval. Also in the LPR zone at 4867 ft. are a few anomalous pyrite features shaped like two semi-circles that are <1 cm in length. The contact of the LPR zone with the next interval was placed along a 1 cm thick pyrite band. The upper Woodford section (4859–4838 ft.) is identified here as the upper pyrite-rich (UPR) zone. This zone contains

disseminated silt to sand-sized pyrite and pyrite nodules, but lacks the pyrite laminae evident in the LPR. Pyrite bands are not common in the UPR, but do occur at 4844, 4851, and 4855 ft. (Figure 4-1). The pyrite nodules are spherical, less than 1 cm in diameter, and occur singularly or in groups. Color changes from black to dark gray, was noticeable when the core is wet, and occurs at 4846 and 4848 feet (Figure 4-1).

4.4.2 Physical Properties

Results of the analyses performed by Weatherford laboratories are presented in Table 4-1. Clay content in the Woodford Shale samples ranges from 44 to 66% (Table 4-1). Quartz content averages 24%, pyrite content ranges from 1 to 6% whereas feldspar content averages 10%. The concentration of carbonate minerals ranges from 0 to 10%. Total organic carbon (TOC) content ranges from 1.5 to 8.5 percent (Table 4-1). The brittleness index, which is a measure of the volumetric fraction of rigid grains as part of the entire volume of the rock matrix (Herwanger et al., 2015), averages 29 (Table 4-2).

The lower Woodford zone has bulk density averaging 2.48 g/cc and grain density between 2.68 and 2.72 g/cc. Magnetic susceptibility is between 6 and 12 m^2/g, specific surface area is between 151 x 10^{-6} and 186 x 10^{-6}, and total iron ranges from 4 to 5 percent of the total rock mass. Water, oil and gas saturations range from 67-74%, 22-28% and 3-9%, respectively.

Well logs were run by Weatherford, and relevant curves include gamma ray, spectral gamma ray, resistivity, neutron porosity, and density porosity. Spectral gamma-ray logs (Figure 4-2) indicate that the elevated gamma count of the Woodford section is

due to high Uranium content. The lower part of the Woodford core has consistently high resistivity averaging 12 ohmm relative to the upper part averaging 7 ohmm. Neutron and density porosity values are highest between 4845 and 4857 ft., which is also where gamma count and TOC content are highest. Bounding this interval, for comparison, are strata with the lowest neutron-density porosity, gamma, and TOC values.

4.4.3 Nuclear Magnetic Resonance Relaxation

Only a single T_2 peak was observed for each echo time in all the samples. The T_{2ML} value at long t_E relaxed slower than both the short and average t_E. The values of the short t_E range from 0.7 to 1.2 ms, whereas the values for the long t_E range from 1.7 to 6.0 milliseconds. The presence of more than one fluid in a pore can cause overlapping signals, which may result in varying T_2 values at different t_E. For all the samples, T_1/T_2 maps plotted marginally above the 1:1 line and some of the plots are presented in Figures 4-3.

A positive slope in a plot of T_{2ML}^{-1} vs. the square of the echo spacing (t_E^2) may suggest the presence of an internal magnetic field gradient (i.e. $G \neq 0$) (Anand and Hirasaki, 2008; Keating and Knight, 2008; Keating, 2014). A general negative trend for all thirteen samples is indicative of relaxation in the absence of an internal magnetic field gradient (Figure 4-4), and this agrees with the plot of the T_1/T_2 ratio.

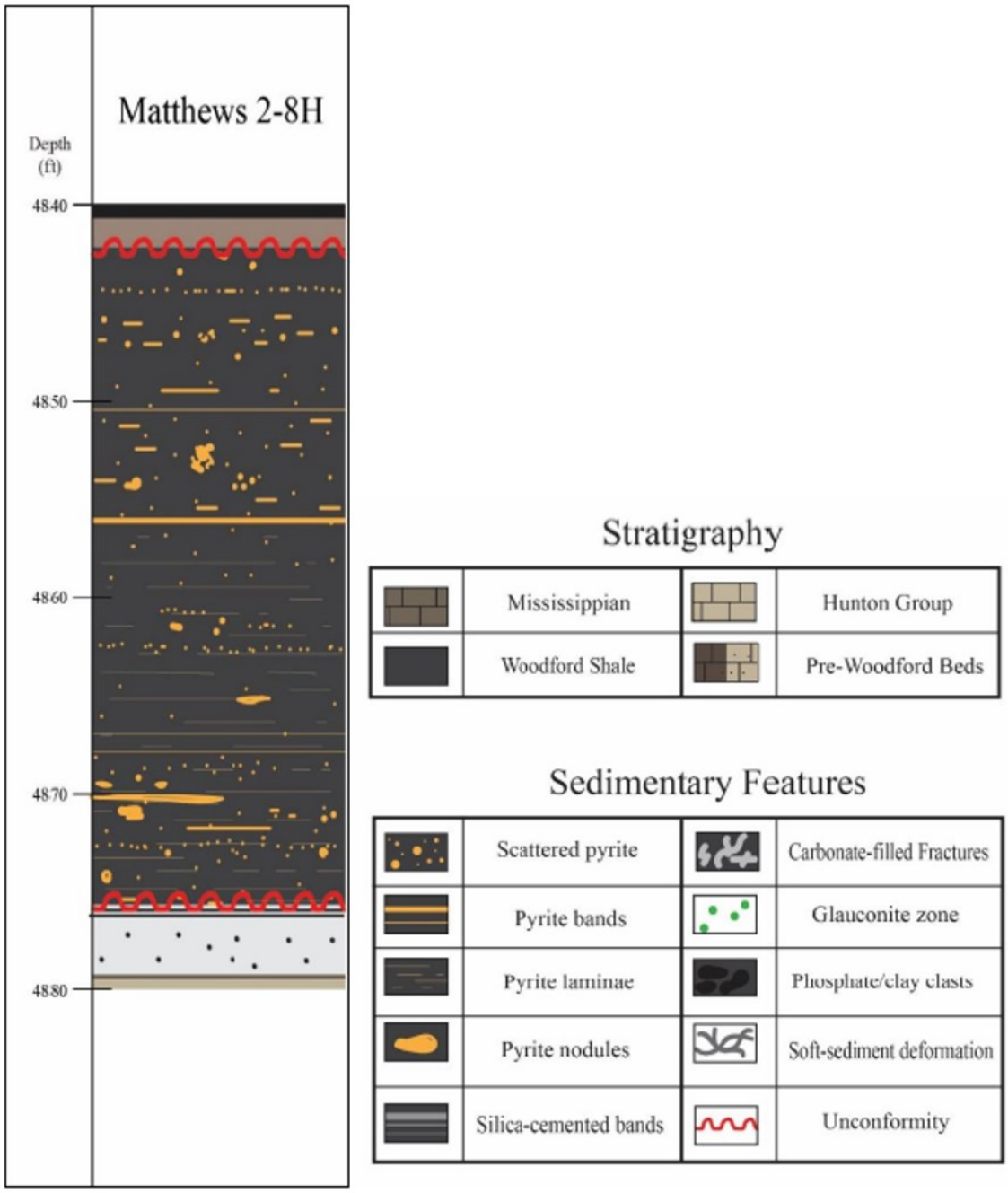

Figure 4-1. Schematic description of lithology and depositional, biogenic, and authigenic features in the Woodford core.

Table 4-1: XRD data of major mineral components from Woodford core in Barber County, Kansas

Core Depth (ft.)	CLAY MINERALS (wt.%)	QUARTZ (wt.%)	CARBONATE (wt.%)	PYRITE (wt.%)	FELDSPAR (wt.%)	TOC (%)
4838	60	26	1	1	11	1.46
4841	61	23	2	2	11	1.55
4844	51	26	8	3	11	2.87
4847	46	28	10	3	11	4.92
4850	66	20	0	1	12	5.31
4853	62	20	1	2	14	6.25
4856	63	17	2	6	12	8.5
4859	44	31	10	3	11	3.54
4862	51	28	8	6	7	3.11
4866	58	24	6	3	8	3.27
4870	55	23	9	4	8	3.14
4871	58	21	6	5	9	3.39
4874	54	21	9	2	9	4.52

Table 4-2: T_{2ML} at long & short t_E, TOC and brittleness index from Woodford core in Barber County Kansas

Core Depth (ft.)	T_{2ML}: Short (msec.)	T_{2ML}: Long (msec.)	Brittleness Index (BI)
4838	1.0	1.8	26.7
4841	0.8	1.8	25.7
4844	0.8	2.0	33.9
4847	0.7	1.9	36.5
4850	0.7	6.0	22.1
4853	0.8	1.7	24.5
4856	1.1	2.4	21.0
4859	1.2	2.4	40.0
4862	1.1	2.5	32.2
4866	1.0	2.1	27.9
4870	1.0	3.2	29.7
4871	0.8	3.0	26.3
4874	1.2	2.5	29.1

Table 4-3: Reservoir properties and percentage iron from Woodford core in Barber County, Kansas

Core Depth (ft.)	Bulk Density (g/cc)	Grain Density (g/cc)	Specific Surface Area (m^2/g)	MS (x 10^{-6} SI) ($\Delta\chi$)	Fe (wt.%)
4862	2.48	2.72	6.0	161	4
4866	2.48	2.71	10.4	181	4
4870	2.48	2.71	12.0	186	4
4874	2.47	2.68	12.0	151	5

Table 4-4: Petrophysical and more reservoir properties from Woodford core in Barber County, Kansas

Core Depth (ft.)	Water Saturation % of PV	Oil Saturation % of PV	Gas Saturation % of PV	Porosity % BV	Permeability (nanoDarcy)
4862	67.2	28.1	4.7	8.6	341
4866	67.0	24.4	8.6	8.6	317
4870	74.0	23.2	2.8	8.6	104
4874	70.4	22.4	7.2	8.0	1700

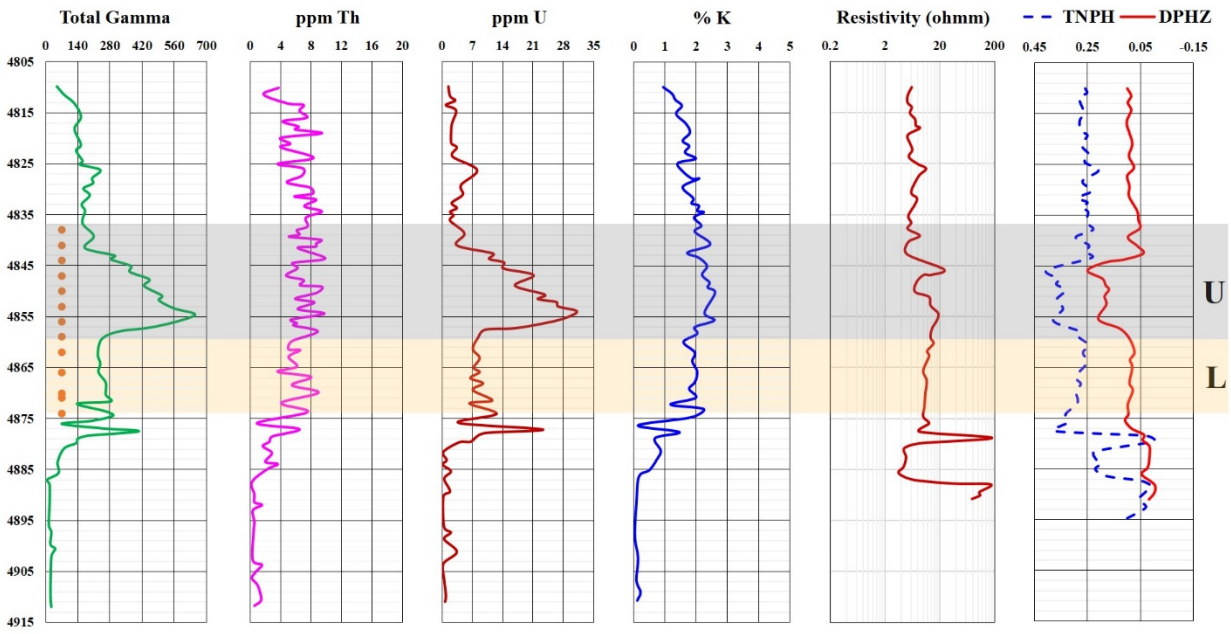

Figure 4-2: Open hole log signatures of the Woodford in south central Kansas. Orange dots in track one indicate the sample points. The solid green curve is the total gamma-ray curve with scale from 0 to 700 GAPI. The solid pink, red and blue curves are for Thorium from 0 to 20 parts per million (ppm), Uranium from 0 to 35 ppm, and Potassium from 0 to 5% in tracks two, three and four respectively. Resistivity log is the solid red curve in track five while the neutron and density logs are in last track in dash blue and solid red curves, respectively. The Light grey highlight delineates the Upper from Lower Woodford zone in the study locality.

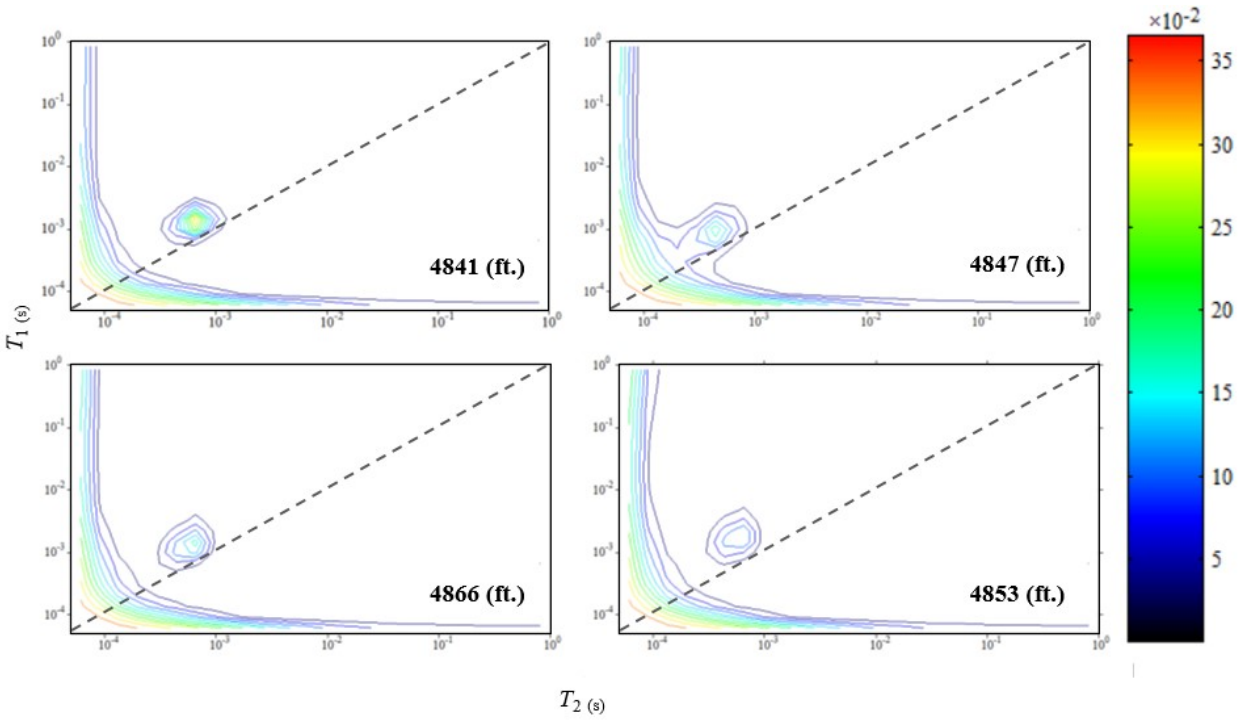

Figure 4-3: T_1/T_2 correlation map for the Woodford. Plots marginally above the 1:1 line indicate absence of magnetic field inhomogeneity in the system. The plots at 4866, 4853, 4847 and 4841 ft. bear similar characteristics to the entire Woodford Shale in the Matthews core and plotted marginally above the 1:1 line. Dashed line is 1:1(unity).

4.5 DISSCUSSION

Variation of the mineralogical composition of shale implies that chemical and mechanical properties will vary. Most producing shale reservoirs tend contain less than 50% clay (Passey et al., 2010; Loucks et al., 2012). Clay minerals, are relatively ductile and stress-sensitive, may influence the S_{por} of pores. And under stress, clay can distort and reduce the volume pore spaces. By contrast, quartz, pyrite, feldspar, and carbonate form rigid particles that support the rock framework. High concentration of these rigid grains may be associated with cluster of larger pores (Loucks et al., 2012). Within the

Woodford study interval, most of the shale contains more than 50% clay. Exceptions are at depths of 4859 and 4847 ft. (Figure 4-5). These clay-dominated intervals are expected to have undergone more compaction and are more chemically and mechanically unstable than the non-clay dominated intervals. On the other hand, shale containing less than 50% clay has mixed mineralogy of carbonates, feldspars and pyrite, may be more brittle (Figure 4-5B). While carbonate minerals may enhance brittleness of rocks, they may typically reduce pores when they are present as cementation materials (Loucks et al., 2012). Both intervals (4859 and 4847 ft.) correspond to the zones with highest brittleness index in the core (Figure 4-5A). In addition, the ratio of thorium-to-potassium (Th/K) (Figure 4-6), which gives insight into the geochemical maturity and degree of compaction of sediments (Hassan et al., 1976), plotted from spectral gamma ray open hole logs indicate no significant variation in geochemical maturity or compaction throughout the core. The plot of brittleness index vs. total clay gives further insight into the mineralogical variation across depth (Figure 4-5A). The interval from 4847 to 4838 ft. contains clay content and brittleness index similar to that observed between 4874 and 4859 ft. These two zones have a more brittle character that may facilitate effective hydraulic fracturing.

4.5.1 Nuclear Magnetic Resonance Characterization

The T_1/T_2 map plots marginally above the 1:1 line is indicative of absence of extra transverse relaxation induced by internal magnetic field gradient. However, the small deviations from the 1:1 line may be due to noise and the limitations of the inversion

algorithm. The absent extra relaxation is probably due to low to negligible magnetic susceptibility contrast between the pore fluids and grains (Table 4-1). This assertion is corroborated by the plot of T_{2ML}^{-1} vs. (t_E^2) which resulted in a negative slope (i.e. $G = 0$) and is indicative of the absence of diffusion relaxation, which if present, may speed up relaxation with increasing t_E (Song et al., 2002). This is not the case as the T_{2ML} measured in the Woodford is larger at long t_E than at short t_E. The values of T_{2ML}^{-1} are determined by the equation $T_{2ML}^{-1} = T_{2S}^{-1} + T_{2B}^{-1} + T_{2D}^{-1}$, but $T_{2D}^{-1} = 0$ and the magnetic susceptibility contrast between the pore fluid and grains is negligible. Surface relaxation will be the dominant relaxation mechanism in a geologic material with negligible magnetic susceptibility (Grunewald and Knight, 2009), which in our case, the expression for T_{2ML}^{-1} is reduced to

$$T_{2ML}^{-1} = T_{2S}^{-1} = \rho_2 \left(\frac{S}{V}\right). \tag{28}$$

Paramagnetic impurities on pore surfaces are capable of enhancing the surface relaxivity ρ_2 (Foley et al., 1996; Bryar et al., 2000). However, this effect is expected to be insignificant based on the reasons stated above.

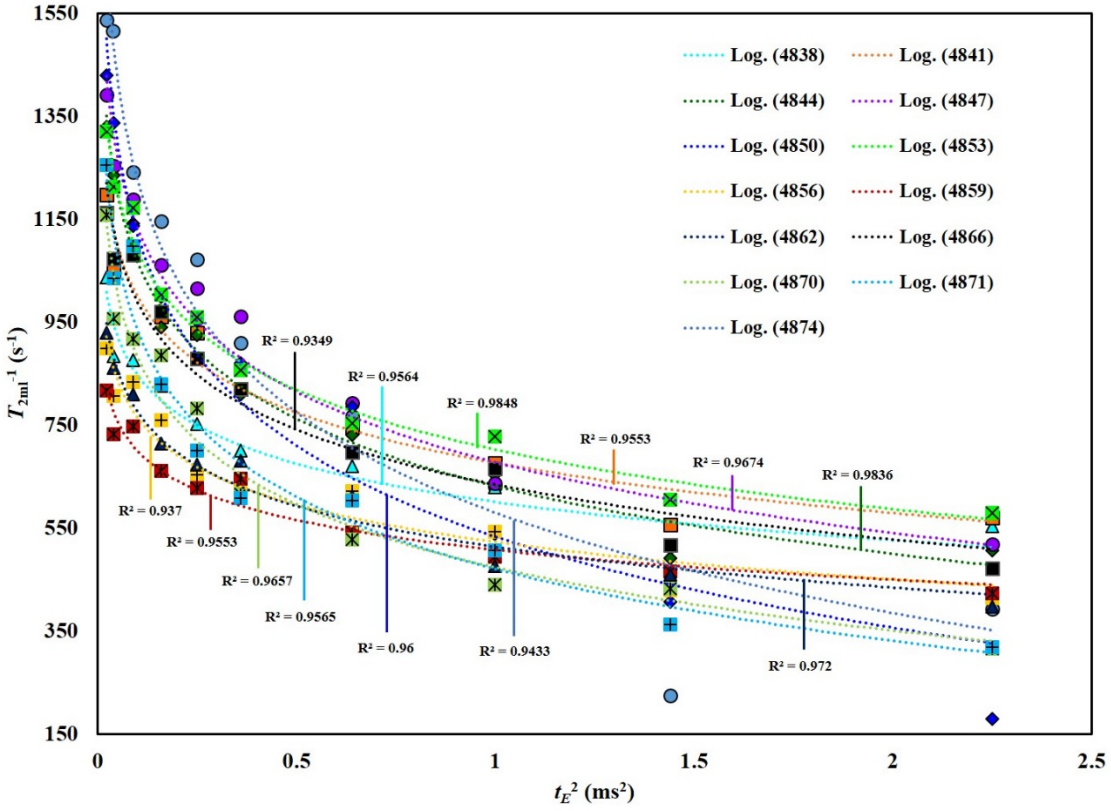

Figure 4-4: Plot showing the dependence of T_2 relaxation on echo spacing t_E, for the Woodford core from Barber County, Kansas.

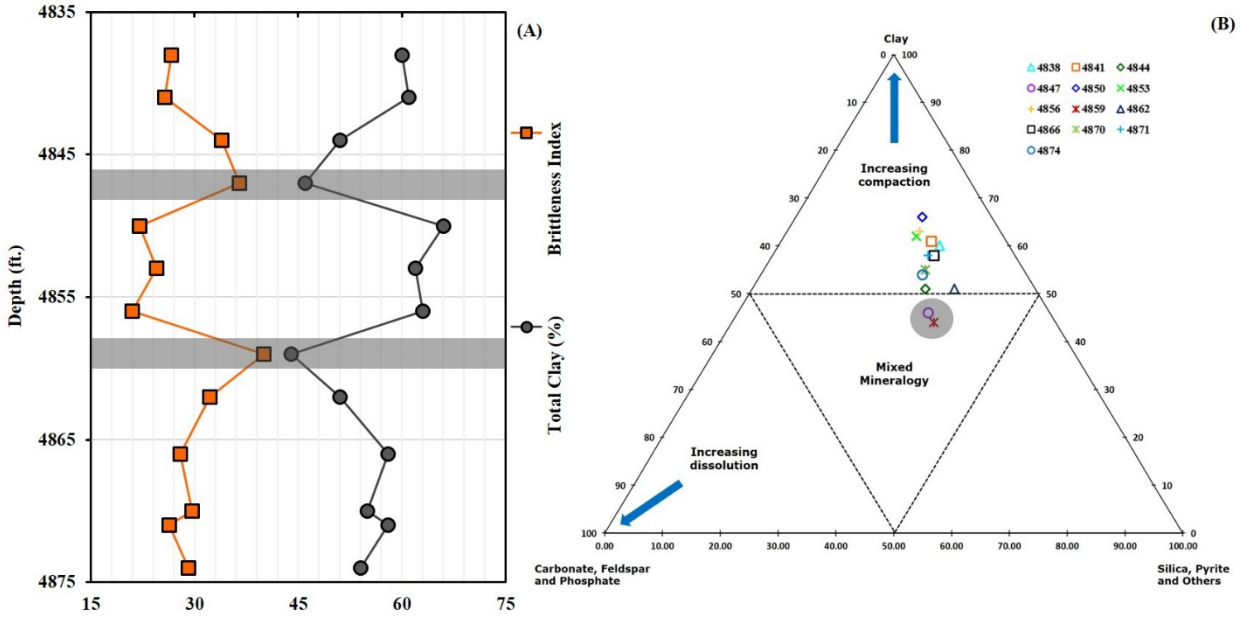

Figure 4-5: (A) Comparative plot between total clay and brittleness index across the Woodford Shale core from Barber County, Kansas. **(B)** Mineral compositional diagram showing stability relationships between end member minerals in the Woodford core from Barber County, Kansas (modified from Loucks et. al. (2012).

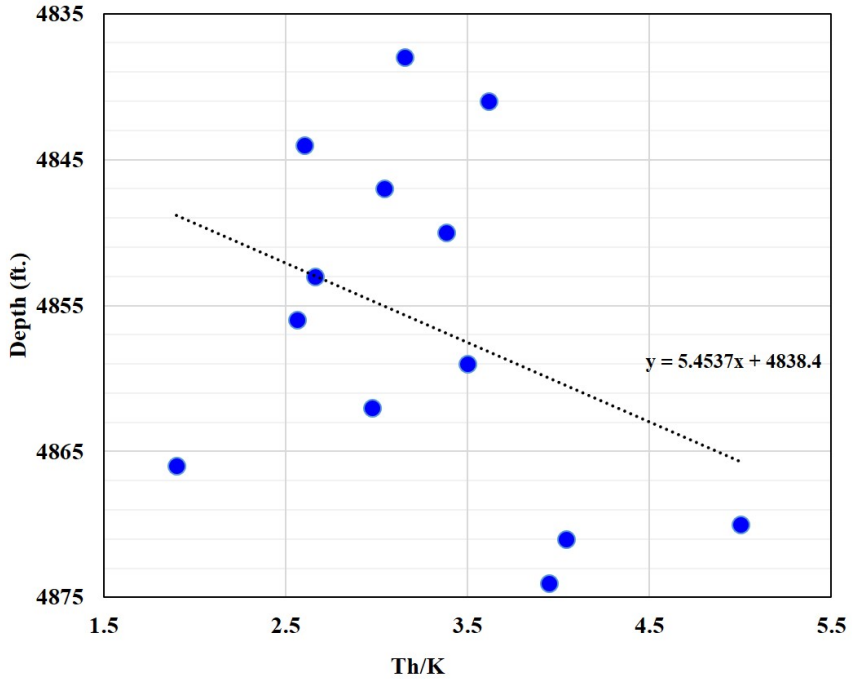

Figure 4-6: Geochemical maturity plot of Th/K ratio in the Woodford Shale core.

The T_{2ML}^{-1} values were plotted at short and long t_E and the general observation was increase in both values in the lower Woodford zone than in the upper zone. T_2 relates to the total number of hydrogen nuclei present within the pore which is used for porosity estimation (Kenyon et al., 1995; Keating and Knight, 2006), whereas the $T_{2ML}^{-1} = \rho_2 (S/V)$ relationship links NMR relaxation rate to permeability (Timur, 1969). A lower T2 value typically reflects the relative size of smaller pores while higher T_2 values corresponds directly to larger pore signals (Grunewald and Knight, 2009). At 4850 ft., the T_{2ML}^{-1} value at long t_E was significantly larger than for the entire interval. This sample also has the highest quantity of total clay in the interval. All clays have hydroxyl groups (OH^-) in their crystal structure that affect measurements of neutron porosity (Passey et

al., 2010). In addition, large amounts of clay-bound water (i.e., capillary bound water or clay adsorbed water), can lead to erroneous estimation of water saturation (S_w) (Eslinger and Pevear, 1988; Passey et al., 2010). The significantly high T_{2ML}^{-1} value at long t_E may be due to the clay effect so described above which is not expected to be part of producible porosity. This contention again raises the argument in favor of either T_{2ML}^{-1} or T_2 cut-off value in determining producible or moveable porosity and as input parameter in the two permeability estimator equations, Timur-Coates or SDR (Timur, 1968a, b; Timur, 1969; Coates and Dumanoir, 1973; Kenyon et al., 1988; Kleinberg and Boyd, 1997; Sezginer et al., 1999; Allen et al., 2001).

In many geologic materials, where ρ_2 varies with mineralogy, it is logical to assume that pore surfaces are compositionally or morphologically heterogeneous (Keating and Knight, 2010). The ρ_2 within the lower Woodford zone, although low, showed minimal variations, which may favor the presence of a more Fe^{2+} over Fe^{3+} rich mineralogy. The spin number for Fe^{2+} is less than that for Fe^{3+} and will result in lower ρ_2 for Fe^{2+}-bearing minerals than for Fe^{3+}-bearing minerals (Keating and Knight, 2010). This supports the description of the Woodford as being deposited under oxygen-deficient conditions, that favored organic matter preservation and allowed iron to be present in reduced state as Fe^{2+} (Cardott and Lambert, 1985; Arthur and Sageman, 1994). This contention is supported by visible iron sulfide (pyrite) in core samples (Figure 4-1) and XRD data shown in Table 4-1.

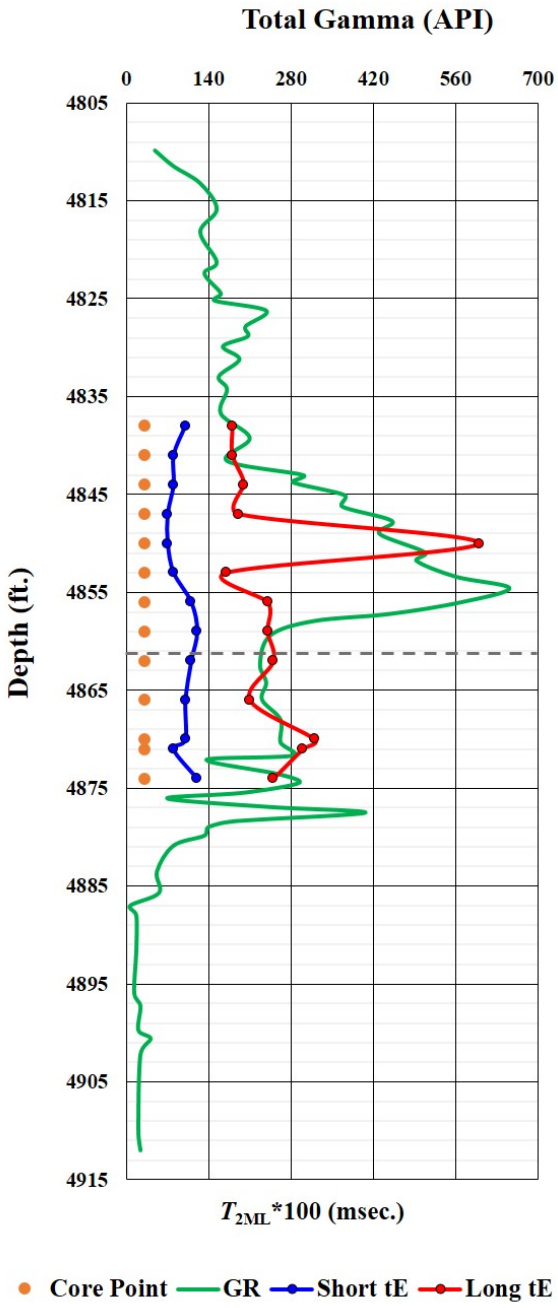

Figure 4-7: The comparative plot of T_{2ML} at long (red curve) & short (blue curve) t_E across the Woodford core from Barber County, Kansas.

Table 4-5: Surface Relaxivity ρ, and Pore Volume to Surface V_p/S, values at average Echo Spacing across Lower Woodford core from Barber *County, Kansas*

Core Depth (ft.)	ρ (μm s^{-1})	V_p/S (nm)
4862	0.50	8.0
4866	0.35	4.6
4870	0.10	1.3
4874	0.15	2.3

The effective hydraulic radius R, of the reservoir's pore system, which is defined as the ratio of the pore volume V_p to the grain fluid interfacial area S, which is an input parameter for permeability estimation equations i.e., $R = V_p/S$ (Goode and Sen, 1988) (Table 4-5). These hydraulic radii are a measure of the distance a proton has to travel to reach a paramagnetic site (Keating and Knight, 2010). The small hydraulic radius or short distance to paramagnetic site indicated by the value of V_p/S in supports the fast T_2 relaxation measured in the Woodford as well as the low porosity and nanoDarcy permeability typical of the lower Woodford zone.

4.6 CONCLUSIONS

This research reviewed petrophysical data provided by Weatherford Laboratories for a Woodford Shale core from Barber County, Kansas. The data described a potential reservoir rock, which was partitioned into upper and lower zones based on chemical, trace element concentrations, clay mineral concentrations mechanical stability, the

brittleness index, and reservoir quality exhibited by the zone labeled as the Lower Woodford than the Upper zone.

NMR measurements obtained from the core to provide a superior approach to characterizing reservoir, showed no evidence of relaxation in the presence of an internal magnetic field gradient. Although surface relaxation was determined to be the dominant relaxation mechanism, the low value and minimal variation in the surface relaxivity is validated by the presence, and quantity of a more Fe^{2+} rich mineralogy in the Woodford zone.

Finally, values of T_{2ML}^{-1} (at both long and short t_E), which are indexed to porosity, generally increased in the zone described as the Lower Woodford compared to the Upper Woodford. The small hydraulic radii or short travel distance of protons to paramagnetic sites were determined to be reasonable given the observed enhanced relaxation of the T_2 time, and measured low porosity and permeability values obtained for the Lower Woodford.

All observations summarized above provide a new insight into the Woodford Shale in Barber County Kansas as a good candidate for further resource evaluation.

REFERENCES CITED

Acholla, F. V., and Orr, W. L., 1993, Pyrite removal from kerogen without altering organic matter: the chromous chloride method: Energy & fuels, v. 7, no. 3, p. 406-410.

Allen, D., Boyd, A., Massey, J., Fordham, E., Amabeoku, M., Kenyon, W., and Ward, W., The practical application of NMR logging in carbonates: 3 case studies, *in* Proceedings SPWLA 42nd Annual Logging Symposium2001, Society of Petrophysicists and Well-Log Analysts.

Allen, D., Flaum, C., Ramakrishnan, T., Bedford, J., Castelijns, K., Fairhurst, D., Gubelin, G., Heaton, N., Minh, C. C., and Norville, M. A., 2000, Trends in NMR logging: Oilfield Review, v. 12, no. 3, p. 2-19.

Anand, V., and Hirasaki, G. J., 2008, Paramagnetic relaxation in sandstones: Distinguishing T 1 and T 2 dependence on surface relaxation, internal gradients and dependence on echo spacing: Journal of magnetic resonance, v. 190, no. 1, p. 68-85.

Arthur, M. A., and Sageman, B. B., 1994, Marine black shales: depositional mechanisms and environments of ancient deposits: Annual Review of Earth and Planetary Sciences, v. 22, no. 1, p. 499-551.

Bachman, H., Crary, S. F., Heidler, R., Vigne, L., Aldan, J., and Akkurt, R., Porosity Determination from NMR Log Data: The Effects of Acquisition Parameters, Noise, and Inversion, *in* Proceedings SPE Annual Technical Conference and Exhibition2007, Society of Petroleum Engineers.

Bloembergen, N., E. M. Purcell, and R. V. Pound, 1948, Relaxation effects in nuclear magnetic resonance absorption: Physical review, v. 73, p. 679

Brownstein, K. R., and Tarr, C., 1979, Importance of classical diffusion in NMR studies of water in biological cells: Physical Review A, v. 19, no. 6, p. 2446.

Bryar, T. R., Daughney, C. J., and Knight, R. J., 2000, Paramagnetic effects of iron (III) species on nuclear magnetic relaxation of fluid protons in porous media: Journal of magnetic resonance, v. 142, no. 1, p. 74-85.

Cardott, B. J., and Lambert, M. W., 1985, Thermal maturation by vitrinite reflectance of Woodford Shale, Anadarko basin, Oklahoma: AAPG Bulletin, v. 69, no. 11, p. 1982-1998.

Cardott, B.J., 2012, Thermal maturity of Woodford Shale gas and oil plays, Oklahoma, USA:
International Journal of Coal Geology, v 103, p. 109-119

Coates, G. R., and Dumanoir, J. L., A new approach to improved log-derived permeability, *in* Proceedings SPWLA 14th Annual Logging Symposium1973, Society of Petrophysicists and Well-Log Analysts.

Coates, G. R., L. Xiao, and M. G. Prammer, 1999, NMR logging: principles and applications, Gulf Professional Publishing.
Daughney, C. J., Bryar, T. R., and Knight, R. J., 2000, Detecting sorbed hydrocarbons in a porous medium using proton nuclear magnetic resonance: Environmental science & technology, v. 34, no. 2, p. 332-337.
Dunn, K.-J., D. J. Bergman, and G. A. LaTorraca, 2002, Nuclear magnetic resonance: petrophysical and logging applications, Elsevier.
Droser, M.L., and Bottjer, D.J., 1986, A semi-quantitative field classification of ichnofabric:
Research method paper: Journal of Sedimentary Research, Vol. 56, no. 4, p. 558-559.
Eslinger, E., and Pevear, D. R., 1988, Clay minerals for petroleum geologists and engineers, Society of Economic Paleontologists and Mineralogis ts.
Foley, I., Farooqui, S., and Kleinberg, R., 1996, Effect of paramagnetic ions on NMR relaxation of fluids at solid surfaces: Journal of Magnetic Resonance, Series A, v. 123, no. 1, p. 95-104.
Gallegos, D. P., Munn, K., Smith, D. M., and Stermer, D. L., 1987, A NMR technique for the analysis of pore structure: application to materials with well-defined pore structure: Journal of colloid and interface science, v. 119, no. 1, p. 127-140.
Goode, P., and Sen, P. N., 1988, Charge density and permeability in clay-bearing sandstones: Geophysics, v. 53, no. 12, p. 1610-1612.
Grunewald, E., and Knight, R., 2009, A laboratory study of NMR relaxation times and pore coupling in heterogeneous media: Geophysics, v. 74, no. 6, p. E215-E221.
Hassan, M., Hossin, A., and Combaz, A., Fundamentals of the differential gamma ray log-interpretation technique, *in* Proceedings SPWLA 17th Annual Logging Symposium1976, Society of Petrophysicists and Well-Log Analysts.
Herwanger, J. V., Bottrill, A. D., and Mildren, S. D., Uses and Abuses of the Brittleness Index With Applications to Hydraulic Stimulation, *in* Proceedings Unconventional Resources Technology Conference, San Antonio, Texas, 20-22 July 2015, Society of Exploration Geophysicists, American Association of Petroleum Geologists, Society of Petroleum Engineers, p. 1215-1223.
Howard, J. J., Kenyon, W. E., and Straley, C., 1993, Proton magnetic resonance and pore size variations in reservoir sandstones: SPE Formation Evaluation, v. 8, no. 03, p. 194-200.
Hürlimann, M., Matteson, A., Massey, J., Allen, D., Fordham, E., Antonsen, F., and Rueslåtten, H., 2004, Application of NMR diffusion editing as chlorite indicator: Petrophysics, v. 45, no. 05.
Keating, K., 2014, A laboratory study to determine the effect of surface area and bead diameter on NMR relaxation rates of glass bead packs: Near Surface Geophysics, v. 12, no. 2, p. 243-254.
Keating, K., and Knight, R., 2006, A laboratory study to determine the effect of iron oxides on proton NMR measurements: Geophysics, v. 72, no. 1, p. E27-E32.
-, 2008, A laboratory study of the effect of magnetite on NMR relaxation rates: Journal of Applied Geophysics, v. 66, no. 3, p. 188-196.
-, 2010, A laboratory study of the effect of Fe (II)-bearing minerals on nuclear magnetic resonance (NMR) relaxation measurements: Geophysics, v. 75, no. 3, p. F71-F82.

Kenyon, W., 1997, Petrophysical principles of applications of NMR logging: The Log Analyst, v. 38.

Kenyon, W., Day, P., Straley, C., and Willemsen, J., 1988, A three-part study of NMR longitudinal relaxation properties of water-saturated sandstones: SPE formation evaluation, v. 3, no. 03, p. 622-636.

Kenyon, B., Kleinberg, R., Straley, C., Gubelin, G., and Morriss, C., 1995, Nuclear magnetic resonance imaging—technology for the 21st century: Oilfield Review, v. 7, no. 3, p. 19-33.

Kirkland, D.W., Denison, R.E., Summers, D.M., Gormly, J.R., 1992, Geology and organic geochemistry of the Woodford Shale in the Criner Hills and Western Arbuckle Mountains: Oklahoma Geological Survey, Vol. 93, p. 38-69.

Kleinberg, R., 1994, Pore size distributions, pore coupling, and transverse relaxation spectra of porous rocks: Magnetic resonance imaging, v. 12, no. 2, p. 271-274.

Kleinberg, R., and Boyd, A., Tapered cutoffs for magnetic resonance bound water volume, *in* Proceedings SPE Annual Technical Conference and Exhibition1997, Society of Petroleum Engineers.

Kleinberg, R., Farooqui, S., and Horsfield, M., 1993a, T_1/T_2 ratio and frequency dependence of NMR relaxation in porous sedimentary rocks: Journal of Colloid and Interface Science, v. 158, no. 1, p. 195-198.

Kleinberg, R., Kenyon, W., and Mitra, P., 1994, Mechanism of NMR relaxation of fluids in rock: Journal of Magnetic Resonance, Series A, v. 108, no. 2, p. 206-214.

Kleinberg, R., Straley, C., Kenyon, W., Akkurt, R., and Farooqui, S., Nuclear magnetic resonance of rocks: T1 vs. T2, *in* Proceedings SPE Annual Technical Conference and Exhibition1993b, Society of Petroleum Engineers.

Kleinberg, R., and Vinegar, H., 1996, NMR properties of reservoir fluids: The Log Analyst, v. 37, no. 06, p. 20-32.

Kleinberg, R. L., and Horsfield, M. A., 1990, Transverse relaxation processes in porous sedimentary rock: Journal of Magnetic Resonance (1969), v. 88, no. 1, p. 9-19.

LaTorraca, G., Dunn, K., and Bergman, D., Magnetic susceptibility contrast effects on NMR T2 logging, *in* Proceedings SPWLA 36th Annual Logging Symposium1995, Society of Petrophysicists and Well-Log Analysts.

Latour, L., Kleinberg, R. L., Mitra, P. P., and Sotak, C. H., 1995, Pore-size distributions and tortuosity in heterogeneous porous media: Journal of Magnetic Resonance, Series A, v. 112, no. 1, p. 83-91.

Levitt, M. H., 2001, Spin dynamics: basics of nuclear magnetic resonance, John Wiley & Sons.

Lewis, R., Ingraham, D., Pearcy, M., Williamson, J., Sawyer, W., and Frantz, J., New evaluation techniques for gas shale reservoirs, *in* Proceedings Reservoir symposium2004, Citeseer, p. 1-11.

Lobza, V., and Schieber, J., 1999, Biogenic sedimentary structures produced by worms in soupy, soft muds: Observations from the Chattanooga Shale (Upper Devonian) and experiments. Journal of Sedimentary Research, v. 69, p. 1041-1049.

Loucks, R. G., R. M. Reed, S. C. Ruppel, and D. M. Jarvie, 2009, Morphology, genesis, and distribution of nanometer-scale pores in siliceous mudstones of the Mississippian Barnett Shale: Journal of sedimentary research, v. 79, p. 848-861.

Loucks, R. G., Reed, R. M., Ruppel, S. C., and Hammes, U., 2012, Spectrum of pore types and networks in mudrocks and a descriptive classification for matrix-related mudrock pores: AAPG bulletin, v. 96, no. 6, p. 1071-1098.

Lowell, S., and J. E. Shields, 2013, Powder surface area and porosity, v. 2, Springer Science & Business Media.

Lüning, S. and Kolonic, S., 2003, Uranium spectral gamma-ray response as a proxy for organic richness in black shales: applicability and limitations: Journal of Petroleum Geology, vol. 26, p. 153-174.

Mercer, G. E., Fitzgerald, S., Day, J., and Filby, R. H., 1993, Determination of organic/inorganic associations of trace elements in kerogen of the New Albany shale: Fuel, v. 72, no. 8, p. 1187-1195.

Müller-Petke, M., Dlugosch, R., Lehmann-Horn, J., and Ronczka, M., NMR Average Pore Size Estimations Outside the Fast Diffusion Regime.

Passey, Q. R., Bohacs, K., Esch, W. L., Klimentidis, R., and Sinha, S., From oil-prone source rock to gas-producing shale reservoir-geologic and petrophysical characterization of unconventional shale gas reservoirs, *in* Proceedings International oil and gas conference and exhibition in China2010, Society of Petroleum Engineers.

Paxton, S.T., Cruse, A.M., Krystyniak, A.M., 2006, Detailed fingerprints of global sea-level change revealed in Upper Devonian-Mississippian Woodford Shale of south-central Oklahoma: American Association of Petroleum Geologists Oral Presentation, Search and Discovery Paper: http://www.searchanddiscovery.com/documents/2006/06095paxton/index.htm?q=%2BtextStrip%3Agamma+textStrip%3Aray+textStrip%3Auranium+textStrip%3Awoodford+- isMeetingAbstract%3Amtgabsyes.

Roberts, C.T., and Mitterer, R.M., 1992, Laminated black shale-bedded chert cyclicity in the Woodford Formation, southern Oklahoma, in K.S. Johnson and B.J. Cardott, eds., Source rocks in the southern Midcontinent, 1990 symposium: Oklahoma Geological Survey, Circular 93, p. 330-336.

Schieber, J., 1998, Sedimentary features indicating erosion, condensation, and hiatuses in the Chattanooga Shale of Central Tennessee: relevance for sedimentary and stratigraphic evolution. In: J. Schieber, W. Zimmerle, and P. Sethi (editors), Shales and Mudstones (vol. 1): Basin Studies, Sedimentology and Paleontology, Schweizerbart'sche Verlagsbuchhandlung, Stuttgart, p. 187-215.

Schieber, J., Krinsley, D., Riciputi, L., 2000, Diagenetic origin of quartz silt in mudstone and implications for silica cycling: Nature, v. 406, p. 981-985.

Senturia, S. D., and Robinson, J., 1970, Nuclear spin-lattice relaxation of liquids confined in porous solids: Society of Petroleum Engineers Journal, v. 10, no. 03, p. 237-244.

Sezginer, A., Mirth, C. C., Van Dort, G., Herron, M., Heaton, N., and Freedman, R., An NMR high-resolution permeability indicator, *in* Proceedings SPWLA 40th Annual Logging Symposium1999, Society of Petrophysicists and Well-Log Analysts.

Song, Y.-Q., Venkataramanan, L., Hürlimann, M., Flaum, M., Frulla, P., and Straley, C., 2002, T 1–T 2 correlation spectra obtained using a fast two-dimensional Laplace inversion: Journal of Magnetic Resonance, v. 154, no. 2, p. 261-268.

Straley, C., Matteson, A., Feng, S., Schwartz, L. M., Kenyon, W. E., and Banavar, J. R., 1987, Magnetic resonance, digital image analysis, and permeability of porous media: Applied Physics Letters, v. 51, no. 15, p. 1146-1148.

Timur, A., Effective porosity and permeability of sandstones investigated through nuclear magnetic resonance principles, *in* Proceedings SPWLA 9th Annual Logging Symposium1968a, Society of Petrophysicists and Well-Log Analysts.

-, An investigation of permeability, porosity, and residual water saturation relationships, *in* Proceedings SPWLA 9th annual logging symposium1968b, Society of Petrophysicists and Well-Log Analysts.

Timur, A., 1969, Pulsed nuclear magnetic resonance studies of porosity, movable fluid, and permeability of sandstones: Journal of Petroleum Technology, v. 21, no. 06, p. 775-786.

Ulmishek, G.F. and Klemme, H.D., 1990, Effective petroleum source rocks of the world: Stratigraphic distribution and controlling depositional factors: AAPG Bulletin, vol.75, p. 1809-1851.

Washburn, K. E., 2014, Relaxation mechanisms and shales: Concepts in Magnetic Resonance Part A, v. 43, no. 3, p. 57-78.

Washburn, K. E., Birdwell, J. E., Seymour, J. D., Kirkland, C., and Vogt, S. J., Low-field nuclear magnetic resonance characterization of organic content in shales, *in* Proceedings SCA Proc SCA2013-002, Society of Core Analysts Symposium, Napa Valley, CA, USA2013.

Wedepohl, K. H., 1971, Environmental Influences on the chemical composition of shales and clays: "*Physics and Chemistry of the Earth, 8,* pp. 307-333

Westphal, H., Surholt, I., Kiesl, C., Thern, H. F., and Kruspe, T., 2005, NMR measurements in carbonate rocks: Problems and an approach to a solution: Pure and Applied Geophysics, v. 162, no. 3, p. 549-570.

Whittall, K. P., M. J. Bronskill, and R. M. Henkelman, 1991, Investigation of analysis techniques for complicated NMR relaxation data: Journal of Magnetic Resonance (1969), v. 95, p. 221-234.

Zhang, G. Q., Hirasaki, G. J., and House, W. V., Diffusion in internal field gradients, *in* Proceedings International Symposium of the Society of Core Analysts, Paper1998, Volume 23.

CHAPTER 5

SUMMARY OF RESEARCH AND FUTURE WORK

This thesis is designed to interpret the effects of paramagnetic minerals on the determination of pore-size distribution in shale using NMR and the implications for estimating permeability.

In chapter 2, based on the models put forward by Kleinberg and Vinegar (1996), G. Q. Zhang et al. (1998, 2003), Hürlimann (1998), and Anand and Hirasaki (2008), the pore geometry was defined as well as the magnitude of the internal gradients, pore size distribution was characterized, and secular relaxation regimes were categorized. Internal magnetic field gradient was determined to dominate the tool gradient, whereas all of the minerals were computed as having small pore except celadonite and montmorillonite. The implication of these classifications is that T_{2ML} shifted to faster time, which may result in the overestimation of *BFV*, which when used as input parameter into permeability equation, and thus, will lead to underestimation of NMR permeability.

In chapter 3, the effects on compaction on NMR T_2 relaxation was determined by considering four common clay minerals, including montmorillonite, glauconite, illite and chamosite mixed with brine and compacted to simulate reservoir conditions. NMR signal

was observed to progressively decay at a faster relaxation rate, to shorter times as compaction, and pore volume-to-surface-ratio, increased.

In chapter 4, the outcome of the analyses carried out in chapters 2 and 3 were applied in order to improve on petrophysical interpretation of the Woodford Shale core from Barber County, Kansas. NMR measurements obtained from the core showed no evidence of relaxation in the presence of an internal magnetic field gradient, and although surface relaxation was determined to be the dominant relaxation mechanism, the low value and minimal variation in the surface relaxivity is validated by the presence, and quantity of a more Fe^{2+} rich mineralogy in the Woodford zone.

The results of our study underscores the need to modify the approach of petrophysical interpretation of shale reservoirs using transverse T_2 relaxation time, however, it should not serve as a definitive guide. Further experimental and simulation work are required because of the wide range of heterogeneities associated with shale. It is recommended that the workflow from this research be ran on multiple unconventional reservoir rocks in order to quantify the internal gradients and determine the critical point and magnetic mineral concentration at which internal gradients become problematic. Secondly, it is recommended that several compaction stages be measured and quantified so as to determine the critical point where compaction diminishes the reservoir quality, and finally, open-hole NMR logging is recommended for integrated reservoir appraisal.

REFERENCES CITED

Anand, V., and G. J. Hirasaki, 2008, Paramagnetic relaxation in sandstones: Distinguishing T 1 and T 2 dependence on surface relaxation, internal gradients and dependence on echo spacing: Journal of Magnetic Resonance, v. 190, no. 1, p. 68–85, doi:10.1016/j.jmr.2007.09.019.

Hu¨rlimann,M.D.,1998, Effective gradients in porous media due to susceptibility differences: Journal of Magnetic Resonance, v. 131, no. 2, p. 232–240, doi:10.1006/jmre.1998.1364.

Kleinberg, R. L., and H. Vinegar, 1996, NMR properties of reservoir fluids: Log Analyst, v. 37, p. 20–32.

Zhang, G. Q., G. J. Hirasaki, and W. V. House, 1998, Diffusion in internal field gradients: Proceedings of the 1998 International Symposium of the Society of Core Analysts, The Hague, The Netherlands, September 14–16, 1998, SCA-9823, 10 p.

Zhang, G. Q., G. J. Hirasaki, and W. V. House, 2003, Internal field gradients in porous media: Petrophysics, v. 44, p. 422–434.

VITA

Christian Chijindu Obasi

Candidate for the Degree of

Doctor of Philosophy

Thesis: EFFECTS OF PARAMAGNETIC MINERALS ON PORE-SIZE DISTRIBUTION IN SHALE

Major Field: Geology

Biographical:

Education:

Christian Chijindu Obasi completed the requirements for the Doctor of Philosophy in Geology at Oklahoma State University, Stillwater, Oklahoma in December 2018.

Christian Chijindu Obasi completed the requirements for the Master of Science in Geology at Temple University, Philadelphia, Pennsylvania in 2008.

Christian Chijindu Obasi completed the requirements for the Bachelor of Science in Geology at University of Nigeria Nsukka, Enugu, Nigeria in 2003.

Experience:
Christian Chijindu Obasi worked at Schlumberger Technology Limited as a Geologist and Petrophysicist for 6 years, immediately after completing his Master of Science degree at Temple University. It was at Schlumberger that he developed interest in nuclear magnetic resonance characterization of unconventional resource plays.

Professional Memberships:
American Association of Petroleum Geologists
Geological Society of America
Society of Sedimentary Geology
Journal of Magnetic Resonance